

Fifth Symposium on
Preclinical Nuclear Imaging
London
28 October 2024



TABLE OF CONTENTS

	Page
GREETINGS	2
PROGRAMME	4
ABSTRACTS	
Oral communications (O 01 – O 12)	8
Keynote lecture (O 13)	30
Poster presentations (P 01 – P 21)	33
SERVICE SECTION	
Internet access	72
PNI TEAM	
PNI organising committee	73
ENDORSEMENT AND SPONSORSHIP	
Endorsement	74
Sponsors	74

GREETINGS

DEAR COLLEAGUES AND FRIENDS

Welcome to the Fifth Symposium on Preclinical Nuclear Imaging (PNI)!

It is a great pleasure to welcome you to King's College London. After a successful meeting last time in Kingston-upon-Hull, we are very pleased to welcome this conference back to London.



It is excellent timing to host PNI 2024 at King's College London, following on from the week when we have installed and validated the first of our two Total-Body PET clinical scanners, which provide the next significant milestone in our translational pathway. Following a successful joint bid from Imperial College and King's College London to the Medical Research Council, a Siemens Quadra (106 cm field-of-view) was installed at St Thomas' Hospital in October 2024. We have also been supported by King's College London to purchase a second Quadra scanner. The EPSRC-funded MITHRAS programme has had continued success in radiopharmaceutical development, while more exciting opportunities have been created, not least through UK government support, such as the Medical Radionuclide Innovation Programme, which enables King's College London to deliver the first robust, scalable UK production route for the PET isotope iodine-124. The latter programmes extend the range of radionuclides available for both clinical and preclinical research in the UK and map onto the upgrade of our GE PETtrace 880 cyclotron to the automated solid target platform. Importantly, preclinical nuclear imaging research at King's College London saw a major boost through recent facility refurbishments with SPECT/CT and PET/CT capabilities upgraded to the latest Mediso Scanners with support from the MRC. Radiopharmaceutical development at King's College London is also supported by existing major Cancer Research UK-funded multi-institution centres.

We are really excited about the future of nuclear imaging and nuclear medicine in the UK and feel the science represented at PNI 2024 covers the full breadth of topics that are of current importance for preclinical nuclear imaging. There are a range of themes covered, spanning a wide arch from new very flexible methodology to attach radioisotopes to diagnostic and therapeutic targeted molecules, via exploiting the powers of nuclear imaging to better understand disease biology, to the clinical applications of radiolabelled probes and theranostics. A particular highlight in the latter domain is the keynote lecture from Prof Margret Schottelius.

We are proud to have exciting scientific contributions including oncology and immunology, imaging cardiovascular disease, metabolism, and the brain. New applications such as supramolecular radiotracers represent exciting pathways for future developments, not least for multi-isotope imaging. We are sure that you will find the programme very interesting and take advantage of a long-awaited opportunity to network and catch up with old friends!

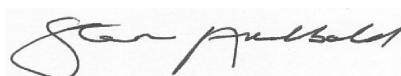
We would also like to deeply thank our sponsors who have made this meeting possible through their generous contributions. They provided a wonderful level of support that has allowed us to run this meeting with minimal registration fees.

We would like to encourage you to visit their booths and learn what new exciting things they have available for you to develop and speed up your research. Last but not least, we would also like to specifically thank the European Society for Molecular Imaging for supporting PNI 2024 and are proud to be endorsed by the leading society in this field.

We wish you a fabulous and joyful day full of exciting science at King's College London! Please do not hesitate to engage with the operational team and organisers if we can help you in anyway on your visit.



Dr Gilbert Fruhwirth



Prof Steve Archibald

PROGRAMME

INTRODUCTION

Chairs *Prof Steve Archibald & Dr Gilbert Fruhwirth*

9:30 Registration
 10:00 Welcome address
 10:05 ESMI & youngESMI

SESSION 1

Chair *Dr Gilbert Fruhwirth*

10:15 **O 01** Prof Eric Aboagye
 Imaging cancer vulnerabilities – the road to translation

10:45 **O 02** Ms Ella-May Hards
 Non-invasive imaging of carnitine utilisation in non-small cell lung cancer with [¹⁸F]fluoromethyl carnitine PET

10:55 **O 03** Ms Sarah Harding
 Development of reporter gene-afforded hypoxia fate mapping in fully immunocompetent cancer models

11:05 **Coffee break**

SESSION 2

Chair *Prof Tammy Kalber*

11:35 **O 04** Prof Tim Witney
 Exploiting the vulnerabilities of drug-resistant cancer for imaging and therapy

12:05 **O 05** Mr Dawoud Dar
 From Lab to clinic: imaging PD-L1 for glioblastoma treatment

12:15 **O 06** Dr Peter Gawne
 Investigating a radioimmunotherapy for high-risk neuroblastoma using GD2-targeted ¹⁷⁷Lu-labelled Dinutuximab-beta

SESSION 3

Chairs Prof Tammy Kalber & Prof Steve Archibald

12:30

Poster pitch flash presentations

P 01 Dr Isaline Renard

CageTag: Co^{III}₄L₆ tetrahedral supramolecular cages as a universal platform for radiopharmaceutical development

P 12 Dr Rico Chi Man

Multi-modal *in vivo* imaging for lung cancer tracking

P 02 Dr Rachel Nuttall

New, optimised diphosphine chelator platforms for receptor-targeted Tc-99m and Re-188 radiopharmaceuticals

P 18 Ms Tia Gibson

Imaging-guided development of polysarcosine-based star dendrimers for drug delivery

P 17 Dr Edward Waters

Quantitative *in vivo* detection of mitochondrial and sarcolemmal membrane potential derived from the pharmacokinetics of radiolabelled lipophilic cations

P 13 Ms Mona Farhangi

Imaging chronic cardiovascular disease using hypoxia targeting PET tracers

P 14 Dr Richard Edwards

A cross-modality combination of imaging agents for the detection of atherosclerotic plaques

P 20 Mr Allen Matt Drews

Count rate performance of a PET tracer on a preclinical SPECT system with multipinhole collimators

P 06 Dr Nadja Van-Camp

A roadmap for [¹¹C]BU99008 PET imaging of astrocyte reactivity in rodent models

P 07 Dr Basma Alenezi

PET/CT imaging of blood-brain barrier integrity and inflammatory tracers during Alzheimer's Disease

13:00 **Lunch**
 Poster presentations and networking

SESSION 4

Chair *Dr Kerstin Sander*

14:30 **O 07** Dr Lisa Wells
 Translational applications of molecular and functional imaging in optimisation of the drug discovery pipeline

14:55 **O 08** Dr Truc Pham
In vivo PET imaging of ⁸⁹Zr-labelled natural killer cells and the modulating effects of a therapeutic antibody

15:05 **O 09** Dr Stephen Paisey
 CageTag: Toward the development of a universal platform for nuclear imaging

15:15 **O 10** Dr Benedetta Arno
 Translational research in radiopharmaceutical development: an industry perspective in navigating the frontiers of therapeutic innovation

15:40 **O 11** Dr George Keeling
 Development of elastin and tropoelastin PET tracers for molecular imaging of atherosclerosis

15:50 **O 12** Mr John Wright
 Preclinical quantitative total body dynamic planar scintigraphy using ^{99m}Tc- and ¹⁶¹Tb-based radiopharmaceuticals

16:00 **Coffee break**

SESSION 5

Chair *Dr Gilbert Fruhwirth and Prof Steve Archibald*

16:30 **O 13** Prof Margret Schottelius
 Theranostic radiopharmaceuticals: lost in translation?

17:30 Prizes and meeting close

18:00 **Drinks reception**

The most advanced radio-TLC scanner available

The Scan-RAM 2™ ensures precise and reproducible results for radiochemical purity measurements and more. Five configurations are available for a wide range of nuclear medicine applications.

This next-generation model builds upon the reliability and success of its predecessor, offering enhanced counting efficiency and a range of innovative features.

Controlled via the industry-standard radiochromatography software, Laura™, the Scan-RAM 2™ provides a flexible and compliant solution.

For further information or to book a demonstration contact our office.

Adjustable interchangeable collimator

New compact design

Occupying less bench space, the new design enables greater flexibility and maximises the available space in your lab.

LAN/USB-C connectivity

Scanning options for optimal results

Speed, maximum count rates and scanning time can all be easily configured.

New smart detectors

Cableless smart detectors offer a new detection technology providing improved performance and usability compared to traditional PMT detectors.

Effective contamination control

A flush, toughened glass surface is easy to clean for effective contamination control.

Detector identification

LED strip changes colour to match that of the detector in use, enabling quick and easy identification.

Magnetised TLC strip plate

Magnetic TLC plates for strips up to 5 x 20 cm can be accommodated on the bed which is securely placed for consistent scanning. They are easily cleaned, conveniently stored, and ideal for lowering finger exposure.

Built-in analogue to digital converter

Converting signals from various HPLC detectors (UV, ECD, etc.) into digital format for integration within Laura™. All signals are consolidated into a single, unified platform.

 **LabLogic**
EXPERIENCE & EXPERTISE

LabLogic Systems Limited
Innovation House, 6 Europa View
Sheffield, S9 1XH, UK

E-mail: solutions@lablogic.com
Tel: +44 (0)114 266 7267

www.lablogic.com

O 01

Imaging Cancer Vulnerabilities – the Road to Translation

E Aboagye

Imperial College London, Department of Surgery and Cancer, GN1, Commonwealth Building, Hammersmith Campus, United Kingdom

eric.aboagye@imperial.ac.uk

Cancers often depend on specific driver oncogenes/tumour suppressors to survive microenvironmental stresses, and this has stimulated efforts to discover and exploit these targets for imaging and therapy. The talk describes PET imaging of metabolic and cell surface markers, the role of pre-clinical imaging, and translation to human imaging. While pre-clinical models may have limitations, they offer opportunities to understand contrasts and pharmacokinetics *in vivo*.

Professor Eric Aboagye – Biography

Eric Aboagye is Professor of Cancer Pharmacology and Molecular Imaging and Director of the CRUK-EPSCRC-MRC-NIHR Comprehensive Cancer Imaging Centre. He joined Imperial College after a PhD at the CRUK Beatson Laboratories in Glasgow, UK and post-doc fellowship at The Johns Hopkins University & Hospital in Baltimore, USA.

His group is interested in the discovery and development of new methods for experimental and clinical cancer molecular imaging. In the past 5 years, the team has invented and translated three novel cancer diagnostics into human application. He has acted as an advisor to GE-Healthcare, GSK, Roche and Novartis. Professor Aboagye was recipient of the 2009 Sir Mackenzie Davidson Medal and was elected as a Fellow of the Academy of Medical Sciences in 2010.

O 02

Non-invasive Imaging of Carnitine Utilisation in Non-small Cell Lung Cancer with [¹⁸F]Fluoromethyl Carnitine PET

E-M Hards¹, RS Edwards¹, HE Greenwood¹, SN Dos Santos¹, R Bielik², SAD Shokry², D Sumpton², DY Lewis², TR Eykyn¹, TH Witney^{1,*}

¹School of Biomedical Engineering and Imaging Sciences, King's College London, St. Thomas' Hospital, London, UK; ²Cancer Research UK Scotland Institute, Glasgow, UK

* tim.witney@kcl.ac.uk

L-Carnitine (LC) is essential for β -oxidation, which is reprogrammed in tumours to support elevated growth and resist treatment [1]. Following uptake via the Na⁺-dependent organic cation transporter-2 (OCTN2), LC transfers free fatty acids across the mitochondrial membrane via carnitine palmitoyltransferase I (CPT1; **Figure 1a**) [2]. Additionally, LC acts as a powerful antioxidant to overcome oxidative stress in the tumour [3,4]. Here, we imaged LC utilisation in tissues and lung cancer for the first time using a fluorine-18 labelled LC derivative, [¹⁸F]fluoromethyl carnitine ([¹⁸F]FMC; **Figure 1b**). Expression of OCTN2 (**Figure 1c**), and [¹⁸F]FMC uptake (**Figure 1d**) were significantly elevated in NSCLC cell lines compared to 16HBE healthy lung epithelial cells, indicating increased LC utilisation in NSCLC. [¹⁸F]FMC uptake correlated with OCTN2 mRNA expression ($R^2=0.644$, $p<0.001$; **Figure 1e**). OCTN2 siRNA knockdown in H1944 cells significantly reduced OCTN2 mRNA expression (**Figure 1f**) and [¹⁸F]FMC uptake by $84.3\pm 2.8\%$ (**Figure 1g**), confirming specificity of [¹⁸F]FMC for OCTN2. Radio-HPLC and ¹⁹F-MRS analysis of NSCLC cells incubated with FMC showed that FMC was conjugated to short-chain fatty acids via CPT1 (**Figure 1i/h**). [¹⁸F]FMC imaging of H1944 tumour-bearing mice revealed rapid extraction from the blood via the kidneys, followed by reabsorption back into the circulation and subsequent uptake by the liver. Excellent tumour-to-background [¹⁸F]FMC images were obtained by PET, which corresponded to high levels of LC and acyl-carnitines (**Figure 1j/k**). These tumours were not avid for [¹⁸F]FDG, which images glucose utilisation. Conversely, H1650 tumours had a glycolytic phenotype and low [¹⁸F]FMC retention (**Figure 1k**). Together, these data highlight the ability to identify distinct metabolic profiles in cancer, which may reveal differential response to treatment.

In conclusion, we have developed a novel PET tracer to image the (patho)physiological utilisation of LC in living subjects, potentially revealing new insights into the metabolic rewiring of tumours. A better understanding of metabolic plasticity has potential implications for patient response and resistance to therapy.

- [1] Harper, M. E. et al. Characterization of a novel metabolic strategy used by drug-resistant tumor cells. *FASEB Journal* 16, 1550-1557
- [2] Longo, N., Frigeni, M. & Pasquali, M. Carnitine transport and fatty acid oxidation. *Biochim Biophys Acta* 1863, 2422-2435
- [3] Li, J. et al. L-carnitine protects human hepatocytes from oxidative stress-induced toxicity through Akt-mediated activation of Nrf2 signaling pathway. *Can J Physiol Pharmacol.* 94, 517-525 (2016)
- [4] Fink, M. A. et al. L-Carnitine-Mediated Tumor Cell Protection and Poor Patient Survival Associated with OCTN2 Overexpression in Glioblastoma Multiforme. *Clin Cancer Res* 25, 2874-2886

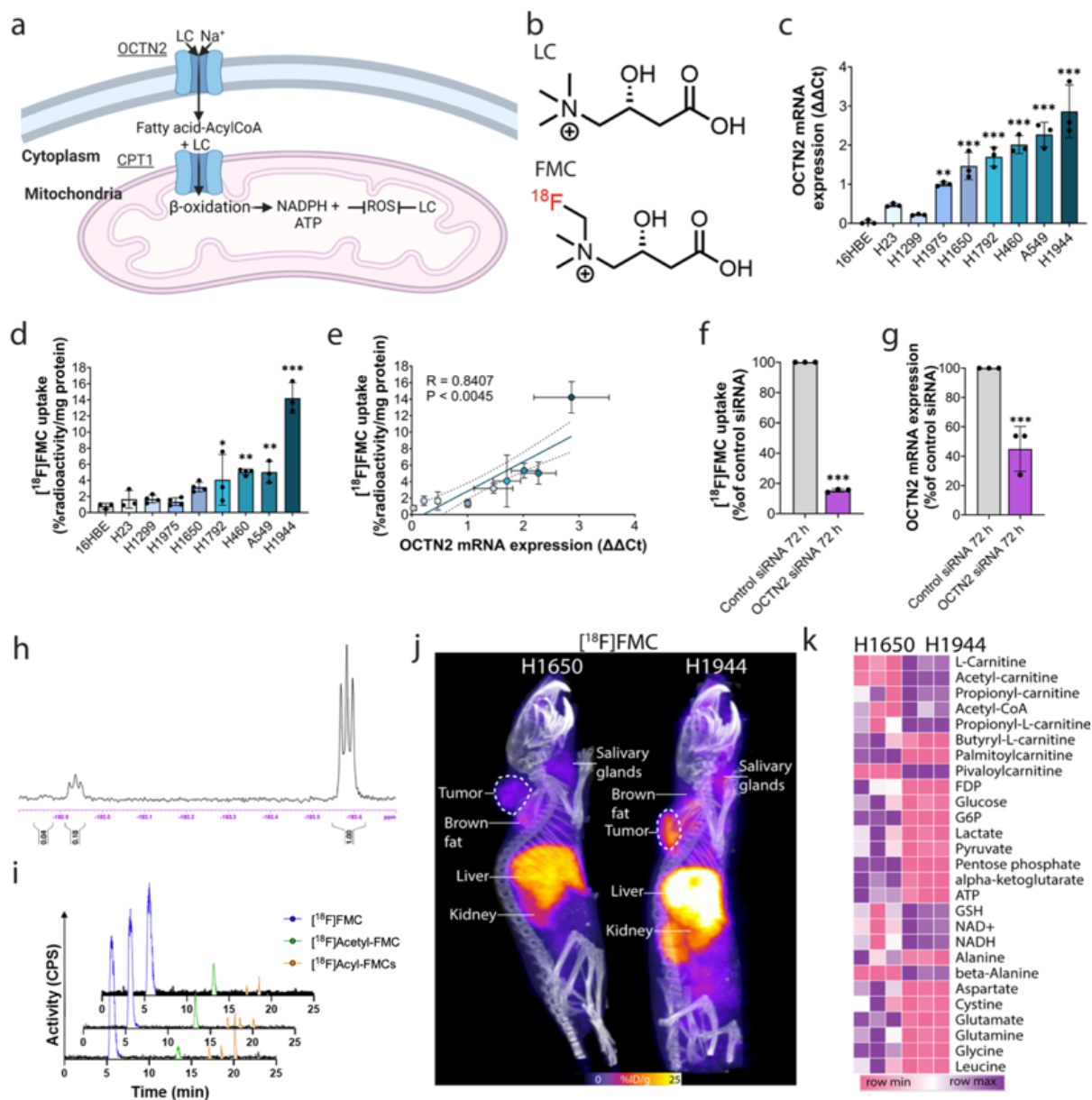


Figure 1. [¹⁸F]Fluoromethyl carnitine ([¹⁸F]FMC) traces LC utilisation via OCTN2 in NSCLC. **a.** Role of LC in B-oxidation and oxidative stress. **b.** Structure of [¹⁸F]FMC and LC. **c.** OCTN2 mRNA expression in cell lysates. Fold change is plotted against an RNA reference (n=3). **d.** Cell uptake of [¹⁸F]FMC in cell lysates 60 min after addition. **e.** Correlation between OCTN2 mRNA expression and [¹⁸F]FMC uptake in panel of NSCLC cell lines. **f.** OCTN2 mRNA levels in H1944 lung cancer cells following 72 h OCTN2 siRNA treatment. **g.** [¹⁸F]FMC cell uptake after 60 min in H1944 lung cancer cells following 72 h OCTN2 siRNA treatment. **h.** NMR spectra in H460 cells following incubation with [¹⁹F]-FMC for 24 h. **i.** HPLC spectra from cell lines incubated with [¹⁸F]FMC. **j.** Representative 120 min maximal intensity projection PET/CT images in a mouse bearing a s/c H1650 and H1944 tumour. **k.** Heatmap illustrating mass spectrometry data from H1650 and H1944 cell lines

O 03

Development of Reporter Gene-afforded Hypoxia Fate Mapping in Fully Immunocompetent Cancer Models

SM Harding*, V Sanz-Moreno, GO Fruhwirth

King's College London and the Institute of Cancer Research, London, UK

* sarah.m.harding@kcl.ac.uk

Tumour hypoxia is an important feature of almost all solid tumours and has been shown to induce a more invasive, immunosuppressive, and treatment-resistant phenotype in cancer cells [1,2]. HIF1 α stabilisation is a robust and widely recognised consequence of hypoxia [2]. Cell populations that experience distinct conditions can be studied using fate-mapping approaches. Here, we use a fate-mapping, multimodal approach to investigate cells that have experienced hypoxia at any point in their life course by triggering a reporter gene switch when cells experience HIF1 α stabilisation.

Employing a viral two-construct approach, we built a detector system to elicit a permanent genetic switch, via Cre/loxP, upon HIF1 α stabilisation. HIF1 α is detected by hypoxia-responsive elements (HRE) that cause Cre expression which turns red fluorescent cells green, manifested by expression of the sodium iodide symporter fused to green fluorescent protein (NIS-GFP), rendering cells traceable *in vivo* by PET or SPECT imaging and identifiable *ex vivo* via fluorescence [3]. KP(B6-F1) lung cancer cells were lentivirally transduced with sensor and reporter constructs and subsequently validated *in vitro* using immunoblotting and immunofluorescence then in C57BL/6 mice.

We generated cells to reflect boundary cases of normoxia and hypoxia by transducing with the reporter construct and enforcing switching with co-expression of constitutive Cre. Both red unswitched "normoxic" and green switched "hypoxic" cell populations established fluorescent tumours subcutaneously, demonstrating suitability of approach for this immunocompetent mouse model (**Figure 1A**). SPECT/CT imaging confirmed NIS-GFP reporter function in line with fluorescence expression (**Figure 1B**). Complete detector expression was achieved by transduction of reporter cells with HRE>Cre sensor. Expression of HRE>Cre was only detectable upon HIF1 α stabilization under hypoxic conditions (1% O₂ 8h) (**Figure 2A**). Cells containing both sensor and reporter constructs effectively induced highly selective reporter switching under 1% O₂ (**Figure 2B**).

We successfully engineered a hypoxia fate-mapping system into lung cancer cells. Extreme conditions have been validated *in vitro* and *in vivo* and the combined fate-mapping system *in vitro*. Next, we will deploy the approach *in vivo* to track cancer cells that have experienced hypoxia at any point during tumour growth in fully immunocompetent mice. Finally exploiting single cell fluorescence for *ex vivo* analyses

- [1] Lu X, Kang Y. Hypoxia and hypoxia-inducible factors: Master regulators of metastasis. (2010) Clin Cancer Res, 16, 5928
- [2] Poon E, Harris AL, Ashcroft M. Targeting the hypoxia-inducible factor (HIF) pathway in cancer. (2009) Expert Rev Mol Med, 11, e26

- [3] Fruhwirth GO, Diocou S, Blower PJ, Ng T, Mullen GE. A whole-body dual-modality radionuclide optical strategy for preclinical imaging of metastasis and heterogeneous treatment response in different microenvironments. (2014) J Nucl Med., 55, 686.

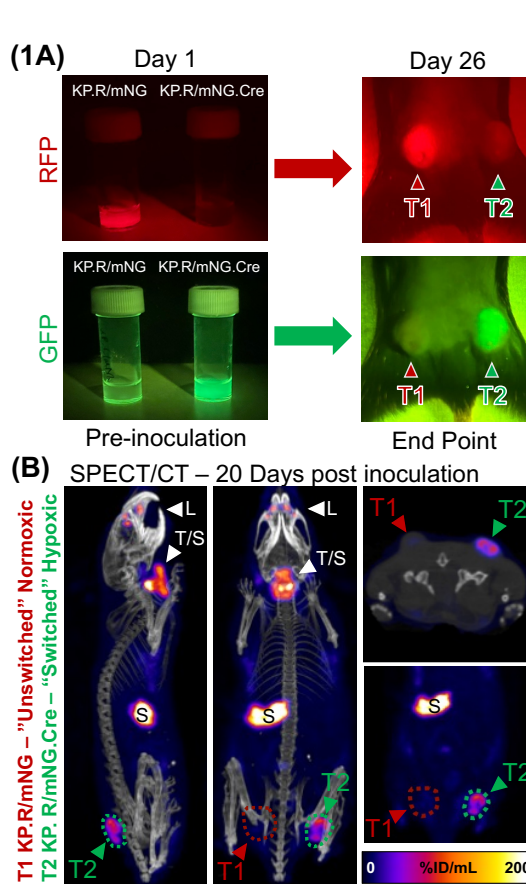


Figure 1. Fluorescent reporter tumours in C57BL/6 mice. **A)** Fluorescence of cancer cells prior to injection on day 1 and maintenance of this fluorescence at end point (day 26). **B)** SPECT/CT of an unswitched "normoxic" KP tumour (T1) and switched "hypoxic" KP tumour (T2) established subcutaneously.

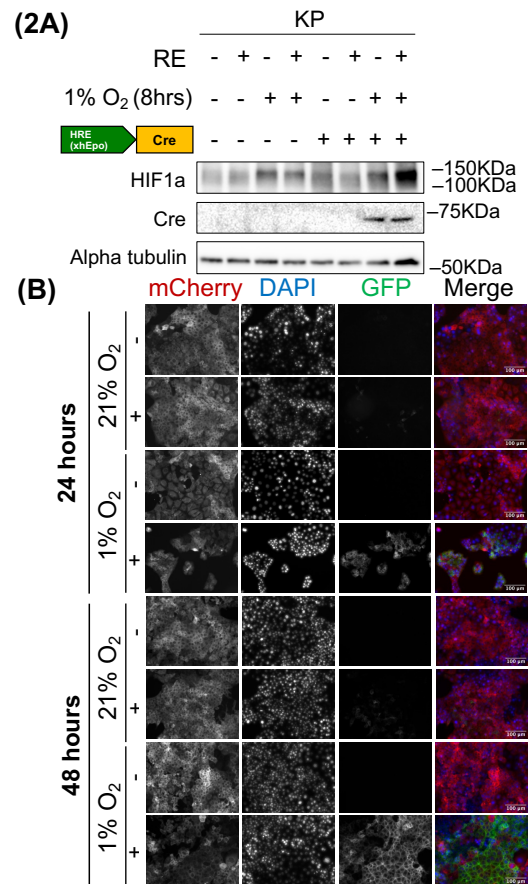


Figure 2. Validation of novel sensor construct. **A)** Expression of sensor construct with and without recombination enhancer (RE) under hypoxia in KP cells. **B)** Ability of sensor to induce reporter switching under hypoxia in KP cells in the presence and absence of RE.

O 04

Exploiting the Vulnerabilities of Drug-resistant Cancer for Imaging and Therapy

TH Witney

School of Biomedical Engineering and Imaging Sciences, King's College London, St. Thomas' Hospital, London, UK

tim.witney@kcl.ac.uk

Therapy resistance is one of the biggest problems currently facing clinical oncology. Despite a revolution in new anti-cancer therapies, durable responses are often not observed due to acquired or innate resistance to these treatment regimens. Currently, there is no satisfactory way to identify patients who are refractive to therapy early in their treatment pathway. As a result, the majority of cancer deaths result from ineffective treatment of therapy-resistant cancer. The early identification of resistance will enable the clinician to dynamically adapt the patient's treatment regimen, with the potential to dramatically improve disease outcomes and provide substantial cost savings for the healthcare system.

Our group is developing a toolbox of molecular imaging agents that bind to biomarkers expressed in therapy-resistant disease. Whilst tumours employ a myriad of different ways to evade death, we have focused our efforts on imaging common downstream pathways that are agnostic to the mechanisms that result in resistance. In this talk, I describe how imaging tumour antioxidant production holds great promise for treatment response monitoring and the prediction of treatment resistance (**Figure 1**). I further describe the development of a novel radiotracer for cancer stem cell imaging in refractive disease. We have exploited the overexpression of these cancer-resistance biomarkers to create novel radionuclide and antibody-drug conjugate therapies. Now, we can not only detect treatment failure but will, in the future, be able to provide an effective treatment option for these patients.

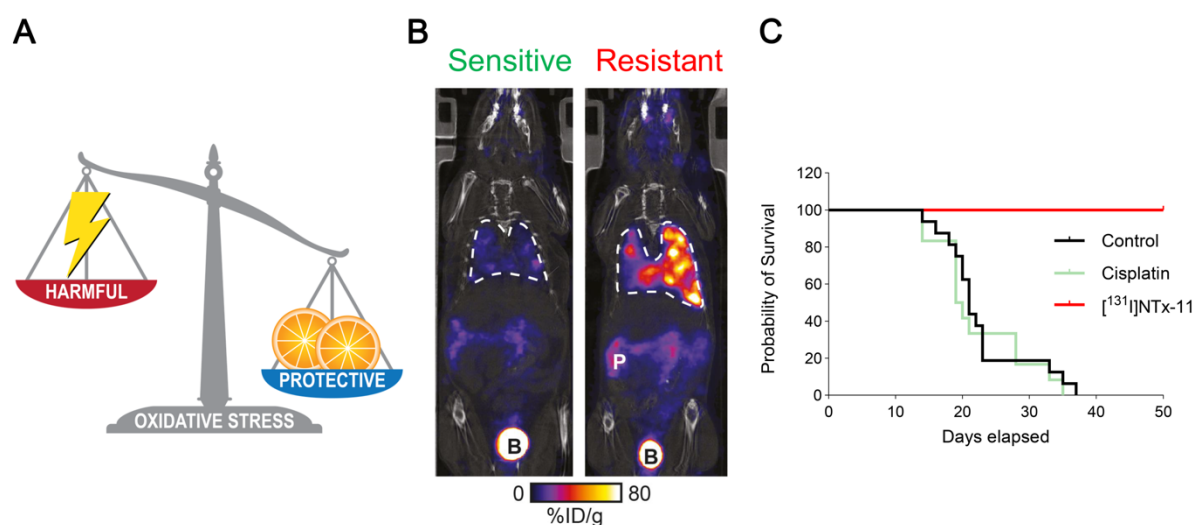


Figure 1. Strategies to diagnose and treat therapy-resistant cancer. **A)** Redox homeostasis provides a surrogate marker of resistance. We have exploited this vulnerability to both image (**B**) and treat (**C**) these highly aggressive cancers.

Professor Tim Witney – Biography



Professor Tim Witney is a Professor of Molecular Imaging and Wellcome Trust Senior Research Fellow at King's College London's School of Biomedical Engineering & Imaging Sciences. His Group, in partnership with other leading researchers, develops next-generation diagnostics to monitor treatment response and identify therapy resistance in cancer. They use pioneering radionuclide therapies to then target the very features that cause refractive disease. He is the co-founder and Chief Scientific Officer at Nuclide Therapeutics and Secretary for the European

Society for Molecular Imaging.

Tim obtained his PhD in Biochemistry from the University of Cambridge in 2010, where he worked in the laboratory of Prof. Kevin Brindle FRS on dynamic nuclear polarisation as a novel method for detecting tumour response to therapy. In 2010, Tim joined the laboratory of Prof. Eric Aboagye at Imperial as a postdoc, developing novel positron emission tomography radiotracers for cancer imaging, before moving to Stanford University in 2013 to work under Prof. Sanjiv Sam Gambhir for further postdoctoral training. In 2015, he established his group at University College London's Centre for Advanced Biomedical Imaging under a UCL Excellence Fellowship and Wellcome Trust & Royal Society Sir Henry Dale Fellowship. He moved to King's College London in 2018 to take up his current post.

O 05

From Lab to Clinic: Imaging PD-L1 for Glioblastoma Treatment

D Dar, M Rodak, C Da Pieve, I Gorczewska, G Sharma, M Niedbala, P Bzowski, E Chmielik, A d'Amico, B Bobek-Bilewicz, E Nowicka, R Tarnawski, W Kaspera, G Kramer-Marek*

The Institute of Cancer Research; Maria Sklodowska-Curie National Research Institute of Oncology; Medical University of Silesia

* gabriela.kramer-marek@icr.ac.uk

Immune checkpoint inhibitors have shown success in reactivating the immune system against many cancers; however, their efficacy has been modest in glioblastoma (GBM) [1]. High programmed death-ligand 1 (PD-L1) expression gives GBM the ability to suppress and evade the immune system [2]. Currently, there is no standardised protocol for the assessment of PD-L1 in GBM. Therefore, we investigated the use of immuno-PET using ^{89}Zr -labelled Atezolizumab to image and measure PD-L1 expression in the preclinical and clinical settings.

The binding affinity and specificity of ^{89}Zr -DFO-Atezolizumab were validated *in vitro*. Mice with orthotopic U87-MGvIII and GL261 tumours received ~ 2 MBq of ^{89}Zr -DFO-Atezolizumab, followed by PET/CT imaging 24, 48, and 72 h post-injection. Radioconjugate biodistribution along with tumour immunophenotyping by immunohistochemistry (IHC) and flow cytometry was assessed *ex vivo*. In the clinical study (NCT05235737), eight newly diagnosed GBM patients treated with/without neoadjuvant pembrolizumab (anti-PD-1) received ~ 37 MBq of ^{89}Zr -DFO-Atezolizumab, followed by PET/CT scans at 48 and 72 h post-injection. Tumour and healthy tissue uptake were quantified (SUVmax), and tumour specimens collected during surgery underwent IHC analysis.

The production of ^{89}Zr -DFO-Atezolizumab was achieved with high radiochemical purity ($>99\%$). *In vitro*, the cell-associated radioactivity of the radioconjugate confirmed PD-L1 expression in the investigated GBM cell lines. In mouse tumour models, ^{89}Zr -DFO-Atezolizumab visualised PD-L1 with high specificity, and its uptake correlated with PD-L1 IHC staining (**Figure 1**). Patients experienced no side effects related to ^{89}Zr -DFO-Atezolizumab. High uptake was observed in patient tumours 48 hours post-injection, although uptake levels varied between patients who had received pembrolizumab and those who had not. The uptake was consistent with PD-L1 expression and T cell infiltration (**Figure 2**).

Our data introduces a novel diagnostic tool for evaluating PD-L1 expression in GBM, with initial findings suggesting that immuno-PET using ^{89}Zr -DFO-Atezolizumab can track dynamic PD-L1 changes within the tumour and lymphoid organs, reflecting systemic alterations induced by neoadjuvant pembrolizumab.

- [1] Waldman AD, Fritz JM, Lenardo MJ. A guide to cancer immunotherapy: from T cell basic science to clinical practice. *Nat Rev Immunol.* 2020; 20(11):651-668.
- [2] Berghoff AS, Kiesel B, Widhalm G, et al. Programmed death ligand 1 expression and tumor-infiltrating lymphocytes in glioblastoma. *Neuro-Oncology.* 2014; 17(8):1064-1075.

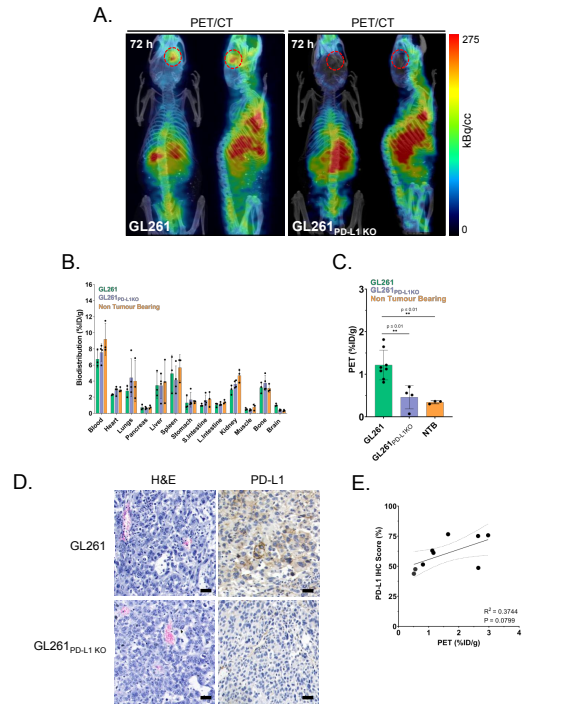


Figure 1. (A) Representative PET/CT images of ⁸⁹Zr-DFO-Atezolizumab uptake at 72 h post-injection in mice-bearing orthotopic GL261 and GL261_{PD-L1} KO tumours. (B) *Ex vivo* biodistribution of mice bearing orthotopic GL261 or GL261_{PD-L1} KO tumours and non-tumour bearing mice 72 h post-injection of ⁸⁹Zr-DFO-Atezolizumab. (C) PET quantification of ⁸⁹Zr-DFO-Atezolizumab tumour uptake in mice bearing orthotopic GL261 or GL261_{PD-L1} KO tumours and non-tumour bearing mouse brain. (D) Representative images of H&E and PD-L1 stained orthotopic GL261 and GL261_{PD-L1} KO tumours (magnification x40; scale bar 10 μm). (E) Correlation coefficient between % positive PD-L1 IHC scoring and ⁸⁹Zr-DFO-Atezolizumab tumour uptake ($R^2=0.3744$).

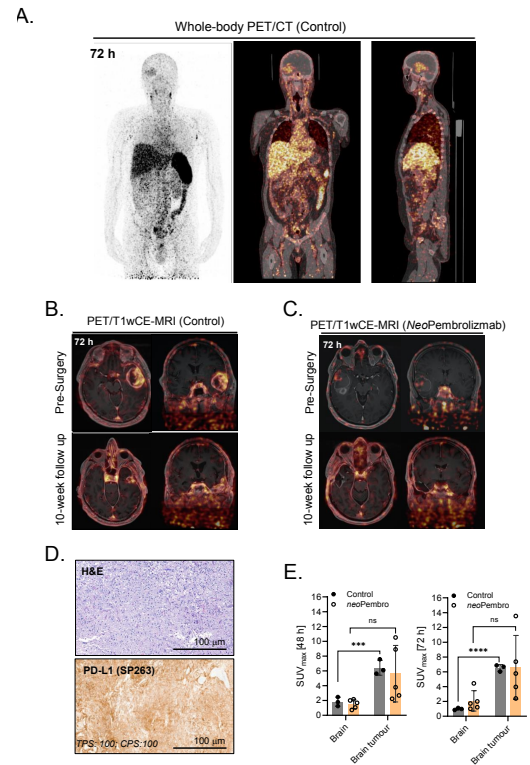


Figure 2. (A) Representative axial and sagittal whole-body PET/CT images of ⁸⁹Zr-DFO-Atezolizumab control patient uptake at 72 h post-injection prior to surgery (B & C) Representative axial and coronal PET/MRI images of ⁸⁹Zr-DFO-Atezolizumab control and neoadjuvant pembrolizumab patient uptake in the brain prior to and 10-weeks post-surgery. (D) Representative images of H&E and PD-L1 IHC stained tissue taken from control patient (from Figure 2B) at the time of surgery. (E) Quantification of ⁸⁹Zr-DFO-Atezolizumab uptake (SUV_{max}) in control (n=3) and neoadjuvant pembrolizumab (n=5) patient healthy brain and brain tumours taken at 48 and 72 h post-injection.

O 06

Investigating a Radioimmunotherapy for High-risk Neuroblastoma using GD2-targeted ¹⁷⁷Lu-labelled Dinutuximab-Beta

PJ Gawne^{1,2,3,*}, J Cleaver², H Blythin², J Cormack², H Schmidt², C Pegrum², JTMM Chupin², S Mather², SYA Terry³, JK Sosabowski², MN Gaze^{1,4}

¹UCL Cancer Institute, University College London, London; ²Centre for Cancer Biomarkers and Biotherapeutics, Barts Cancer Institute, Queen Mary, University of London, London; ³School of Biomedical Engineering and Imaging Sciences, King's College London, London; ⁴Department of Oncology, University College London Hospitals NHS Foundation Trust, London

* p.gawne@ucl.ac.uk

Neuroblastoma is the most common extracranial solid tumour of childhood. In high-risk patients (~50%), the 3-year Event-Free Survival is ~50% [1]. Molecular radionuclide therapy (MRT) using [¹³¹I]MIBG is an established treatment of neuroblastoma. However, target expression and clinical outcomes can be variable. An alternative target is disialoganglioside, GD2 – which is overly expressed on neuroblastomas – and a clinical antibody targeting GD2, Dinutuximab-beta, has improved survival in patients [2]. In this work, we developed a radioimmunotherapy against GD2-positive neuroblastoma using ¹⁷⁷Lu-labelled Dinutuximab-Beta (¹⁷⁷Lu-DB).

Dinutuximab-beta (DB) was conjugated with the bifunctional chelator, p-SCN-Bz-DOTA (**Figure 1A**). The radiochemical yield, purity and stability of ¹¹¹In-DB and ¹⁷⁷Lu-DB was measured using radio-HPLC and iTLC. GD2-binding of ¹⁷⁷Lu-DB was tested using the GD2+ LAN-1 and TAM6 neuroblastoma cell lines. Finally, SPECT/CT imaging and *ex vivo* biodistribution of ¹¹¹In-DB and ¹⁷⁷Lu-DB was performed in mice bearing LAN-1 or TAM6 tumours.

Radiolabelled DB was synthesized with consistently high radiochemical purity (>99%), with high *in vitro* stability (**Figure 1B/C**). The specific binding of ¹⁷⁷Lu-DB to GD2 was confirmed in GD2+ LAN-1 and TAM6 cells; with 27.3±2.1 % and 3.0±1.4% binding, respectively – which could be blocked with excess antibody (**Figure 1D**). *In vivo* SPECT-CT imaging showed higher uptake in LAN-1 tumour ('GD2-high') xenografts compared with TAM6 tumour ('GD2-low') allografts (**Figure 1E**), with 59.6±22.6 %ID/g and 16.1±3.1 %ID/g at 72h p.i. in LAN-1 and TAM6 respectively (**Figure 1F**). Finally, ¹⁷⁷Lu-DB showed high uptake and retention in LAN-1 tumours with 53.8±7.1 %ID/g and 46.1±18.3 %ID/g at 3d and 6d p.i. respectively – with a non-targeted antibody ¹⁷⁷Lu-Rituximab (¹⁷⁷Lu-Rit) showing lower uptake at both timepoints (**Figure 1G**).

In conclusion, the clinically-used GD2-targeting antibody Dinutuximab-beta was successfully radiolabelled with ¹⁷⁷Lu, creating a beta-therapy radiopharmaceutical for high-risk neuroblastoma. ¹⁷⁷Lu-Dinutuximab beta shows specific binding to GD2-positive cell lines and high tumour uptake *in vivo*.

[1] Bagatell et al., *Pediatr. Blood. Cancer*. 2023, 70(Suppl.6), e30572.

[2] Ladenstein et al. *Lancet Oncol*. 2018, 19, 1617–1629

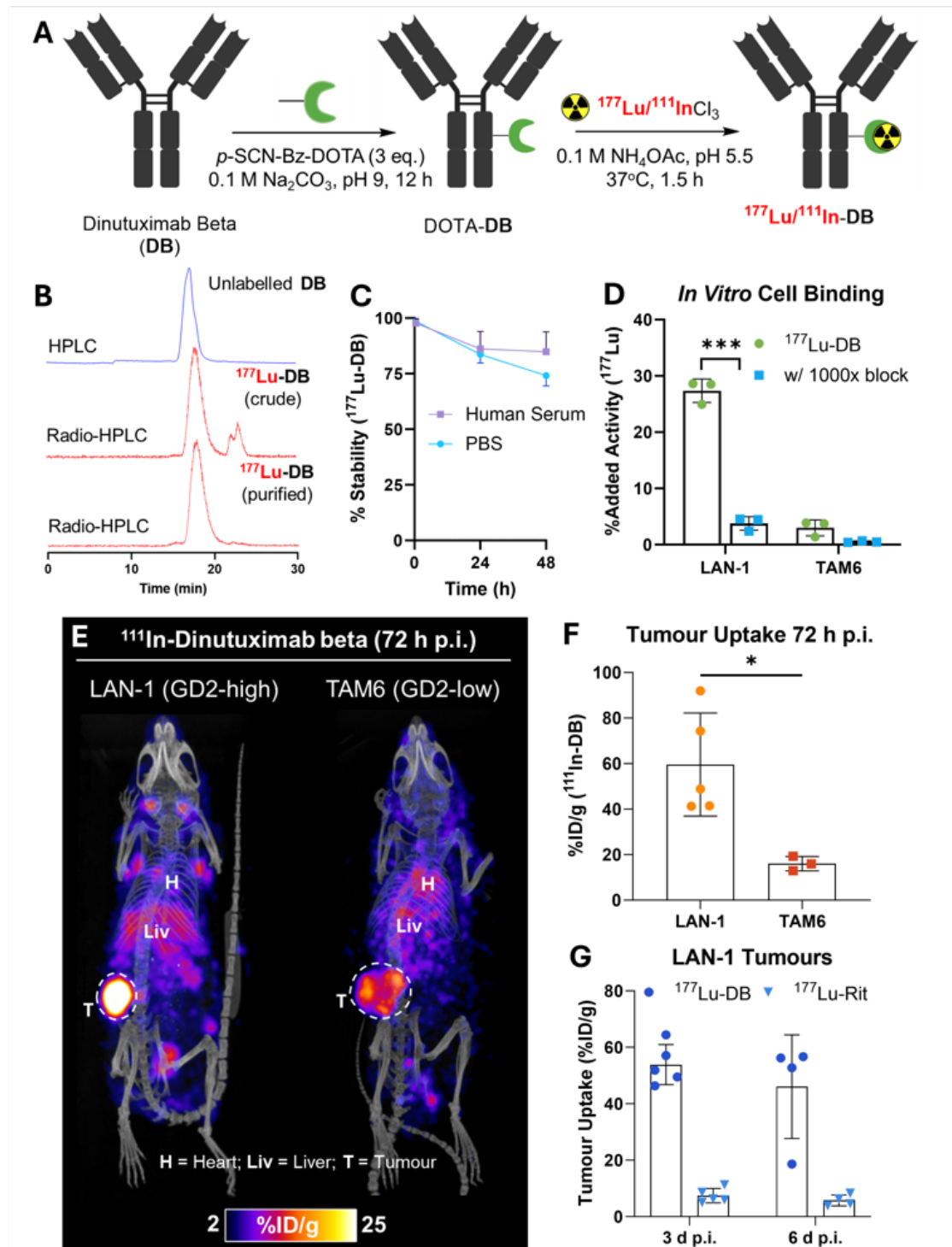


Figure 1. A) Schematic showing the bioconjugation of Dinutuximab beta (DB) with p-SCN-Bz-DOTA and radiochemistry reactions to form ^{177}Lu - and ^{111}In -DB. B) Representative HPLC chromatogram of DB (top graph) & radio-HPLC chromatograms showing radiolabelled ^{177}Lu before (middle graph) and after (bottom graph) size-exclusion purification. C) Stability of ^{177}Lu -DB in 5x excess (v/v) PBS or human serum. D) Cell uptake of ^{177}Lu -DB in LAN-1 (GD2-high) and TAM-6 (GD2-low) cells without a n d with blocking with 1000x excess Dinutuximab beta. E) *In vivo* SPECT-CT maximum intensity projection (MIP) images showing the biodistribution of ^{111}In -DB (10-14 MBq, 40 μg mAb) 72 h after intravenous (i.v.) injection in mice bearing LAN-1 xenografts (left) and TAM6 tumour allografts (right). F) *Ex vivo* tumour uptake of ^{111}In -DB in mice bearing LAN-1 & TAM6 tumours at 72 h post-injection (p.i.) expressed as % injected dose per gram (%ID/g). G) *Ex vivo* LAN-1 tumour uptake of ^{177}Lu -DB and ^{177}Lu -Rituximab (^{177}Lu -Rit), at 3d and 6d post-injection i.v. (%ID/g). * $P > 0.05$; *** $P > 0.001$. All Error bars = Mean +SD.

O 07

Translational Applications of Molecular and Functional Imaging in Optimisation of the Drug Discovery Pipeline

Lisa Wells

VP Translational Pharmacology, Invicro, Burlington Danes, Hammersmith Hospital, London

lwells@invicro.com

The estimated research and development investment needed to bring a new medicine to the market is substantial; for disorders of the nervous system, this equates to an estimated 766 million dollars per new therapeutic agent (median: \$765.9M, 95% CI 323-1473.5M), with 75-88% accounted for by trail failures and only 10% of candidates reaching final approval [1]. Drug development costs increase disproportionately with the phase of drug development, and it is worth noting that the 90% failure rate is for drug candidates that are already advanced to phase I clinical trials, and does not include the drug candidates in the preclinical stages.

Analyses of clinical trial data from 2010 to 2017 show four possible reasons attributed to the 90% clinical attrition rate of drug development: lack of clinical efficacy (40%-50%), unmanageable toxicity (30%), poor drug-like properties (10%-15%), and lack of commercial needs and poor strategic planning (10%) [2]. These observations align with need to apply 'Morgan's Three Pillars of Survival' to the drug discovery pipeline to produce early and robust evidence of tissue exposure, target engagement, and pharmacological activity [3].

The application of imaging techniques to evaluate target binding and therapeutic drug-target occupancy is a powerful tool in drug discovery and has clear utility in answering Morgan's Three Pillars. Here, an overview of the application of the nuclear imaging 'toolbox' to support translational studies is given focusing on:

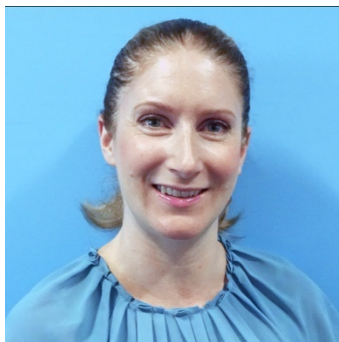
- Therapeutic compound CNS biodistribution applications.
- Current tools to evaluate dose-occupancy study applications in the CNS.
- Pharmacodynamic outcome measures in the absence of direct imaging measures.

[1] JAMA, 2020, 323(9):844-853.

[2] Nat Rev Drug Discov, 2019;18:495e6.

[3] Drug Discovery Today, 2012, 17 (9/10), 419-424.

Dr Lisa Wells – Biography



With over 15 years experience in the field of pharmacology, Dr. Wells's expertise is designing and applying pharmacological techniques from tissue studies to translational PET imaging to evaluate novel radioligands and understand target engagement/ pharmacodynamic outcome measures *in vivo*. She holds a first-class honours degree in medical biochemistry prior to completing a Ph.D. in Neuropharmacology at the University of Surrey.

In 2007, Dr. Wells joined the nuclear imaging field taking a role at GlaxoSmithKline Clinical Imaging Centre where she applied preclinical molecular imaging techniques to support drug discovery and development. Later she transitioned to Head of Biology at Imanova Centre for Imaging Sciences (2011). At Invicro, Dr. Wells uses her knowledge of the pharmaceutical industry to lead the global Discovery CNS Applications, using her expertise to support optimal study design to provide clear study outcomes with a view to translating studies to the clinic.

O 08

***In Vivo* PET Imaging of ⁸⁹Zr-Labeled Natural Killer Cells and the Modulating Effects of a Therapeutic Antibody**

TT Pham*, A Chenoweth, N Patel, A Banu, G Osborn, PJ Blower, SN Karagiannis, MT Ma

King's College London, School of Biomedical Engineering and Imaging Sciences, London, United Kingdom

* truc.pham@kcl.ac.uk

Natural Killer (NK) cells can kill cancer cells via antibody-dependent cell-mediated cytotoxicity (ADCC): a tumour-associated IgG antibody binds to the CD16 receptor of NK cells via the antibody Fc region and activates NK cell cytotoxic functions. Here, we employed PET imaging to assess NK cell migration to HER2-positive HCC1954 breast tumours, examining the influence of HER2-targeted trastuzumab antibody treatment on NK cell tumour accumulation [1].

Human NK cells from healthy donors were expanded *ex vivo* and labelled with [⁸⁹Zr]Zr-Oxine. *In vitro* experiments compared the phenotypic markers, viability, proliferation, migration, degranulation, and ADCC behaviours of both labelled (⁸⁹Zr-) and unlabelled NK cells. Female NSG mice bearing orthotopic human breast HCC1954 tumours were administered ⁸⁹Zr-NK cells alongside trastuzumab or a sham treatment, then PET/CT imaged over 7 days. Flow cytometry and gamma-counting were used to analyse the presence of ⁸⁹Zr-NK cells in liver and spleen tissues.

⁸⁹Zr cell radiolabelling yields measured 42.2±8.0%. At an average specific activity of 16.7±4.7 kBq/10E6 cells, ⁸⁹Zr-NK cells retained phenotypic and functional characteristics including CD56 and CD16 expression, viability, migration, degranulation and ADCC capabilities. *In vivo* PET/CT studies indicated predominant accumulation of ⁸⁹Zr-NK cells in the liver and spleen. *Ex vivo* analyses of liver and spleen tissues indicated that the administered human ⁸⁹Zr-NK cells retain their radioactivity *in vivo* and that ⁸⁹Zr does not transfer to cells of murine soft tissues, thus validating this ⁸⁹Zr PET method for NK cell tracking. Notably, ⁸⁹Zr-NK cells migrated to HER2-positive tumours, both with and without trastuzumab treatment. Trastuzumab treatment was associated with increased ⁸⁹Zr-NK cell signal at days 1 and 3 PI (**Figure 1**).

In vitro, ⁸⁹Zr-NK cells maintained key cellular and cytotoxic functions. *In vivo*, ⁸⁹Zr-NK cells trafficked to HER2-positive tumours, with trastuzumab treatment correlating with enhanced ⁸⁹Zr-NK infiltration. This study demonstrates the feasibility of using PET to image ⁸⁹Zr-NK cell infiltration to solid tumours.

[1] Pham et al (2024). *In Vivo* PET Imaging of ⁸⁹Zr-Labeled Natural Killer Cells and the Modulating Effects of a Therapeutic Antibody. *Journal of Nuclear Medicine*, 65(7), 1035-1042.

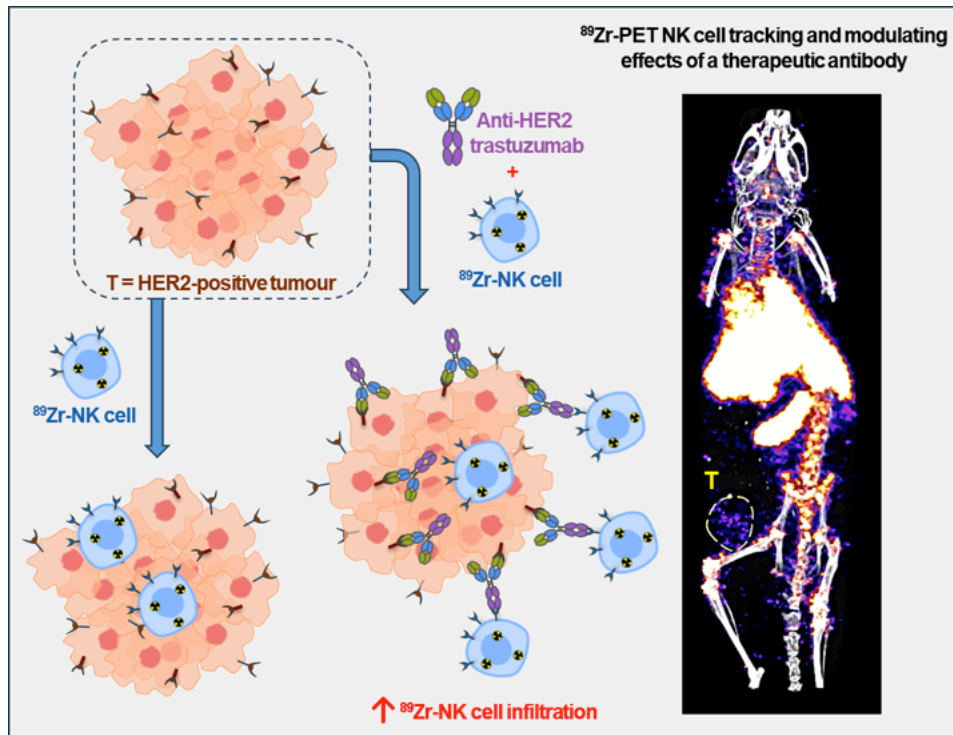


Figure 1. ⁸⁹Zr-Labeled Natural Killer Cells and the Modulating Effects of a Therapeutic Antibody

O 09

Effect of Protein Construct on the Efficiency of Tumour Targeting via the $\alpha\beta6$ Motif – a Comparison of Zr-89 Labelled mAb against a Zr-89 Labelled Streptavidin-Biotin Peptide Construct

SJ Paisey^{1,*}, EA Swift², TJ Phesse³, JF Marshall⁴, PJ Rizkallah⁵, AL Parker², R Bayliss²

¹PETIC, School of Medicine, Cardiff University, Cardiff, CF14 4XN, UK; ²Division of Cancer and Genetics, School of Medicine, Cardiff University, Cardiff, CF14 4XN, UK; ³European Cancer Stem Cell Research Institute, Cardiff University, Cardiff, CF24 4HQ, UK; ⁴Centre for Tumour Biology, Barts Cancer Institute, Queen Mary University of London, London, EC1M 6BQ, UK; ⁵Division of Infection and Immunity, School of Medicine, Cardiff University, Cardiff, CF14 4XN, UK

* paiseysj@cardiff.ac.uk

Here we explore the effect of protein construct on the efficiency of tumour targeting via the $\alpha\beta6$ motif. Mice bilaterally grafted with $\alpha\beta6$ positive and $\alpha\beta6$ negative melanoma cells (A375- $\beta6$ and A375) were serially PET/CT imaged over 140 h with either a Zr-89 labelled $\alpha\beta6$ targeting monoclonal antibody (620W, biotechne) or a biotinylated $\alpha\beta6$ targeting peptide (A20) conjugated to Zr-89 labelled streptavidin. Both agents, the 620W mAb and the streptavidin were labelled with via modifications of established DFO chelator conjugation methods [1,2]. After conjugation of the DFO-chelator the streptavidin was also reacted with succinic acid to reduce kidney trapping *in vivo* [3].

In comparison to the Zr-89-DFO labelled mAb, the Zr-89-DFO labelled streptavidin conjugated peptide exhibited a markedly altered biodistribution pattern, which was dominated by kidney uptake with greatly reduced liver uptake and no obvious spleen uptake. The Zr-89-DFO labelled streptavidin conjugated peptide also exhibited faster pharmacokinetics with peak tumour intensity at 24 hours post injection and peak specific uptake at 48 hours post injection compared to 72 hours and 140 hours for the Zr-89-DFO labelled mAb. Assessment of uptake concentrations (%IA/ml) revealed broadly equivalent peak tumour uptake values for both tracers although the Zr-89-DFO labelled mAb exhibited higher non specific uptake in the negative control tumours (**Figure 1**).

These promising results suggest Zr-89 labelled streptavidin conjugated with biotinylated peptides could provide a useful alternative labelling strategy to the Zr-89 radiolabelling of mAbs particularly when high background spleen or liver uptake is not desired or mAbs raised against the desired target are not available.

- [1] Vosjan, M. J. W. D.; Perk, L. R.; Visser, G. W. M.; Budde, M.; Jurek, P.; Kiefer, G. E.; van Dongen, G. A. M. S. Conjugation and Radiolabeling of Monoclonal Antibodies with Zirconium-89 for PET Imaging Using the Bifunctional Chelate p-Isothiocyanatobenzyl-Desferrioxamine. *Nat. Protocols* 2010, 5 (4), 739–743.
- [2] Knight, J. C.; Paisey, S. J.; Dabkowski, A. M.; Marculescu, C.; Williams, A. S.; Marshall, C.; Cornelissen, B. Scaling-down Antibody Radiolabeling Reactions with Zirconium-89. *Dalton Trans.* 2016, 45 (15), 6343–6347.
- [3] Wilbur, D. S.; Hamlin, D. K.; Buhler, K. R.; Pathare, P. M.; Vessella, R. L.; Stayton, P. S.; To, R. Streptavidin in Antibody Pretargeting. 2. Evaluation of Methods for Decreasing Localization of Streptavidin to Kidney While Retaining Its Tumor Binding Capacity. *Bioconjugate Chem.* 1998, 9 (3), 322–330.

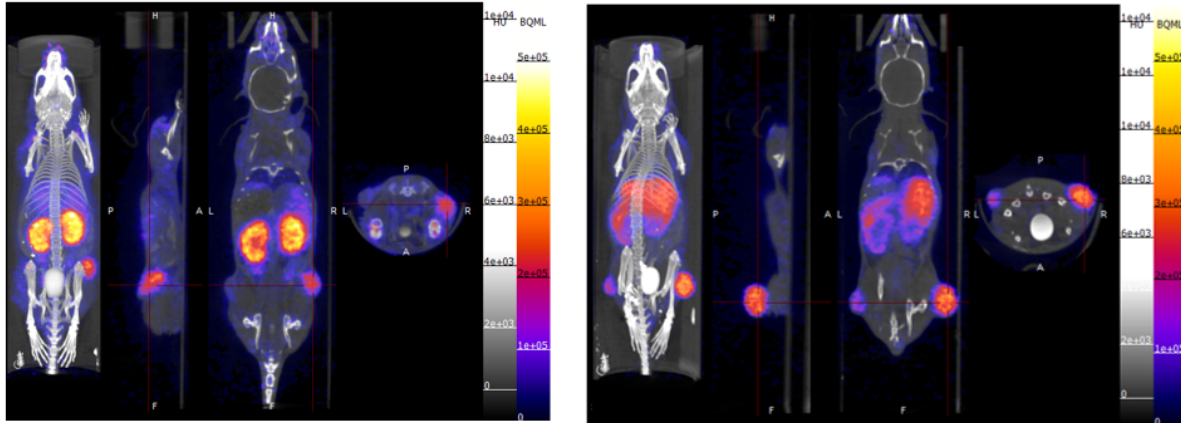
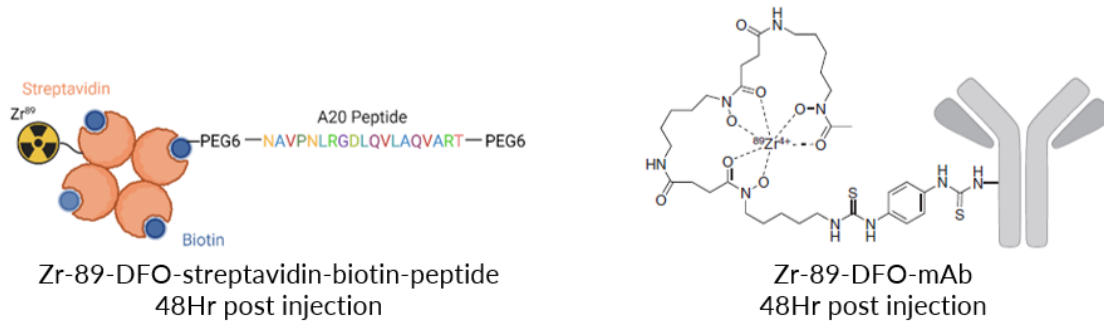


Figure 1. Biodistribution of Zr-89-DFO labelled streptavidin conjugated peptide (**left**) and the Zr-89-DFO labelled mAb (**right**)

O 10

Translational Research in Radiopharmaceutical Development: An Industry Perspective in Navigating the Frontiers of Therapeutic Innovation

B Arno

Medicines Discovery Catapult, Block 35, Mereside, Alderley Park, Macclesfield, Cheshire, SK10 4ZF

benedetta.arno@md.catapult.org.uk

In a quest to address patients need for more personalised and targeted medicines, the theranostic approach of Radiopharmaceutical Therapy (RPT) is gaining lots of traction. Combining a radioactive isotope with a highly specific ligand against different target in tumour cells, radiopharmaceuticals are a great asset for diagnostic and therapeutic purposes.

Thanks to the approval of two RPT agents, Lutathera and Pluvicto, targeting SSTR positive and PSMA positive cancer cells respectively, radiopharmaceuticals have attracted lots of interest and investment in the last 5 years and demonstrated that, contrarily to their predecessors, they can be safe, easy to use and highly efficacious. Unfortunately, despite a rapid market expansion, only a third of preclinically approved drugs enters clinical trials and among them the failure rate is high. Their low success rate has been mainly attributed to lack of preclinical predictability and access to the right skills and technologies.

At Medicines Discovery Catapult, with established radiochemistry protocols and imaging and analytical methods we can assess biodistribution, dosimetry and efficacy of RPT agents in relevant animal models. Presenting a couple of case studies, we will showcase how we can support the preclinical characterization of new radiopharmaceuticals in order to advance their development and facilitate their successful transition into the clinic.

Dr Benedetta Arno – Biography

Benedetta is an expert scientist, with over 12 years of research experience within academia and industry. She has been leading and overseeing in vivo drug discovery projects, applying imaging modalities and ex vivo tissue analysis to characterize distribution and efficacy of many therapeutics, including radiopharmaceuticals, across a variety of diseases and therapeutic areas. She currently works as Lead scientist in Translational Imaging at MDC where she drives the preclinical development of innovative drugs with the ultimate

aim of bringing medicines to patients faster.

Benedetta has a BSc in biotechnology and MSc Hons in biomedical science before completing her PhD in Neuroscience.

O 11

Development of Elastin and Tropoelastin PET Tracers for Molecular Imaging of Atherosclerosis

GP Keeling, A Jones, X Wang, C Carrera, S Padovan, G Digilio, RM Botnar, A Phinikaridou*

King's College London, School of Biomedical Engineering and Imaging Sciences, London, United Kingdom

* alkystis.1.phinikaridou@kcl.ac.uk

Elastin is abundant in healthy vessels whereas its precursor tropoelastin is negligible. Both elastin and tropoelastin accumulate in atherosclerotic plaques [1,2]. We have previously demonstrated tropoelastin-targeted imaging using mono- and tetrameric Gd-based tropoelastin- and monomeric elastin-specific MR agents (TESMA & ESMA respectively) [1–3]. Herein, we report the development of PET analogue probes for imaging of elastin and tropoelastin with a view towards clinical translation.

DOTA analogues of ESMA and TESMA were previously synthesised. A new conjugate of TESMA was synthesised using the chelator tris(hydroxypyridinone) (THP-TESMA). These conjugates were radiolabelled with gallium-68 and labelling conditions were optimised using ITLC and radio-HPLC. *In vivo* evaluation was performed in a mouse model, which involved male ApoE^{-/-} mice fed a high-fat diet undergoing tandem stenosis (TS) of the right carotid artery that develops both stable and unstable atherosclerotic plaques [4]. PET imaging with contrast-enhanced CT was used to investigate the uptake of the tracers in plaques, biodistribution and pharmacokinetics. Excised organs were gamma-counted for further biodistribution data.

Imaging data showed faster blood clearance of both TESMA conjugates compared with DOTA-ESMA. [⁶⁸Ga]Ga-DOTA-ESMA and [⁶⁸Ga]Ga-THP-TESMA showed focal uptake in plaques, while [⁶⁸Ga]Ga-DOTA-TESMA showed less focal uptake throughout the vasculature (**Figure 1**).

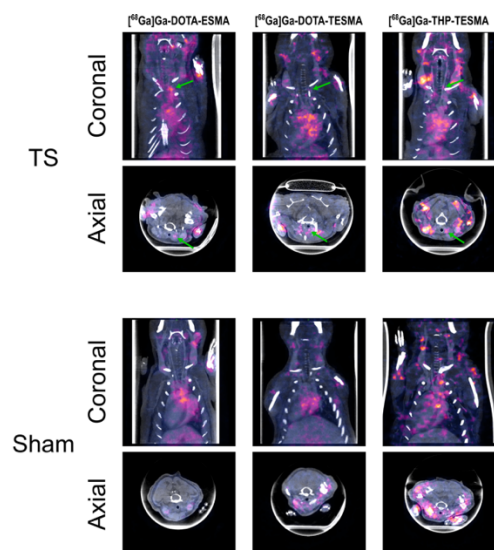


Figure 1. PET/CT images of mice which underwent tandem stenosis (TS) surgery or a sham surgery, 30-40 min post-injection with each PET probe. Mice were pre-injected with a CT contrast agent and were imaged dynamically over 60 min. Green arrows show areas of plaques of interest.

Biodistribution data suggest that the [^{68}Ga]Ga-DOTA-ESMA showed greater uptake than the tropoelastin-targeting probes in the vasculature generally. [^{68}Ga]Ga-DOTA-ESMA and [^{68}Ga]Ga-THP-TESMA accumulated in areas with plaques while [^{68}Ga]Ga-DOTA-TESMA did not show the same level of selectivity.

We have successfully modified and redesigned MR probes to be suitable for PET imaging. Development of (tropo)elastin-specific radiotracers for PET imaging will facilitate clinical translation by overcoming regulatory barriers such as toxicity concerns due to the vastly smaller quantities required than MRI agents. We have shown that (tropo)elastin-targeting agents accumulate in atherosclerotic plaques and we are investigating how this relates to plaque instability.

- [1] Capuana, F, Phinikaridou A, Stefania R, Padovan S, Lavin B, Lacerda S, Almouazen E, Chevalier Y, Heinrich-Balard L, Botnar RM, Aime S and Digilio G, Imaging of Dysfunctional Elastogenesis in Atherosclerosis Using an Improved Gadolinium-Based Tetrameric MRI Probe Targeted to Tropoelastin, *Journal of Medicinal Chemistry*, 2021/ 64, 15250-61.
- [2] Phinikaridou, A, Lacerda S, Lavin B, Andia ME, Smith A, Saha P and Botnar RM, Tropoelastin: A novel marker for plaque progression and instability, *Circulation. Cardiovascular imaging*, 2018/ 11, e007303.
- [3] Lavin, B, Lacerda S, Andia ME, Lorrio S, Bakewell R, Smith A, Rashid I, Botnar RM and Phinikaridou A, Tropoelastin: an in vivo imaging marker of dysfunctional matrix turnover during abdominal aortic dilation, *Cardiovascular Research*, 2020/ 116, 995-1005.
- [4] Chen, YC, Bui AV, Diesch J, Manasseh R, Hausding C, Rivera J, Haviv I, Agrotis A, Htun NM, Jowett J, Hagemeyer CE, Hannan RD, Bobik A and Peter K, A novel mouse model of atherosclerotic plaque instability for drug testing and mechanistic/therapeutic discoveries using gene and microRNA expression profiling, *Circulation Research*, 2013/ 113, 252-65

O 12

Preclinical Quantitative Total Body Dynamic Planar Scintigraphy Using ^{99m}Tc - and ^{161}Tb -based Radiopharmaceuticals

JD Wright^{1,2}, I Renard^{1,2}, IA Middleton³, J Domarkas², E Foyle³, PJ Lusby³, SJ Archibald^{1,2,*}

¹School of Biomedical Engineering and Imaging Sciences, King's College London, 4th Floor Lambeth Wing, St Thomas' Hospital, London, SE1 7EH, UK; ²Centre for Biomedicine and PET Research Centre, Hull York Medical School, University of Hull, Hull, HU6 7RX, UK; ³EaStCHEM School of Chemistry, University of Edinburgh, Joseph Black Building, David Brewster Road, Edinburgh, EH9 3FJ, Scotland, UK

* stephen.archibald@kcl.ac.uk

Dynamic planar scintigraphy using prompt-gamma emitting radionuclides enhances the preclinical imaging workflow of SPECT studies. Accurate quantification of planar scintigraphy frames allows for time activity curves to be generated in support of pharmacokinetic and dosimetry studies. Using a single pinhole collimator on a small animal SPECT/CT scanner, whole-body images of mice can be acquired in a single field of view (FOV) and quantified using sensitivity-based correction factors [1,2]. Quantitative accuracy was demonstrated *in vivo* using [^{99m}Tc]TcO₄⁻ encapsulated supramolecular cage constructs and [^{161}Tb]Tb-PSMA-617 [3,4]. Sensitivity correction resulted in count-rate uniformity across the FOV and returned accurate quantification in phantoms and *in vivo*. 60-second planar frames were acquired over 1-hour post-injection in naïve mice comparing two ^{99m}Tc based radiopharmaceuticals (n=22) and [^{161}Tb]Tb-PSMA-617 in an LNcaP tumour bearing mouse. Whole-body quantification was $99.3 \pm 7.6\%$ (^{99m}Tc) and $94.6 \pm 3.6\%$ (^{161}Tb) of the sensitivity and decay corrected recorded injected doses and was underestimated when quantified without sensitivity correction ($75.0 \pm 7.4\%$ (^{99m}Tc) and $76.6 \pm 3.1\%$ (^{161}Tb)). Animals which underwent ^{99m}Tc SPECT/CT following 1-hour dynamic scintigraphy quantitatively agreed with planar results: $99.5 \pm 10.6\%$ (final frame, planar) vs. $99.1 \pm 5.5\%$ (SPECT). Furthermore, [^{161}Tb]Tb-PSMA-617 uptake to the tumour was established by sensitivity corrected region of interest analysis and was comparable between the final frame of planar scintigraphy (5.2 %ID) and SPECT (5.3 %ID) at 1-hour post-injection (**Figure 1**). Whole-body injected dose and organ specific regions of interest by planar scintigraphy correlates to the recorded injected dose and whole-body SPECT following sensitivity-based correction.

Quantification was reproducibly accurate to within $\pm 10\%$, a threshold previously reported as acceptable for image-based radionuclide dosimetry calculations. The addition of quantitative dynamic planar scintigraphy into the preclinical workflow followed by SPECT imaging adds value to pharmacokinetic and dosimetry studies using SPECT radio-pharmaceuticals.

- [1] Georgiou M, Fysikopoulos E, Mikropoulos K, Fragoageorgi E, Loudos G. Characterization of “ γ -Eye”: a Low-Cost Benchtop Mouse-Sized Gamma Camera for Dynamic and Static Imaging Studies. 2016. 19:398-407
- [2] Bailey D, Hennessy T, Willowson K, Henry E, Chan D, Aslani A, Roach P. *In vivo* quantification of ^{177}Lu with planar whole-body and SPECT/CT gamma camera imaging. 2015. 20 (2015)

- [3] Burke B, Grantham W, Burke M, Nichol G, Roberts D, Renard I, Hargreaves R, Cawthorne C, Archibald S, Lusby P. Visualizing Kinetically Robust CoIII4L6 Assemblies in Vivo: SPECT Imaging of the Encapsulated [^{99m}Tc]TcO₄⁻ Anion. 2018. 140, 49, 16877–16881
- [4] Benešová M, Schäfer M, Bauder-Wüst U, Afshar-Oromieh A, Kratochwil C, Mier W, Haberkorn U, Kopka K, Eder M. 2015. Preclinical Evaluation of a Tailor-Made DOTA-Conjugated PSMA Inhibitor with Optimized Linker Moiety for Imaging and Endoradiotherapy of Prostate Cancer. *The Journal of Nuclear Medicine*. 2015 56 (6) 914-920

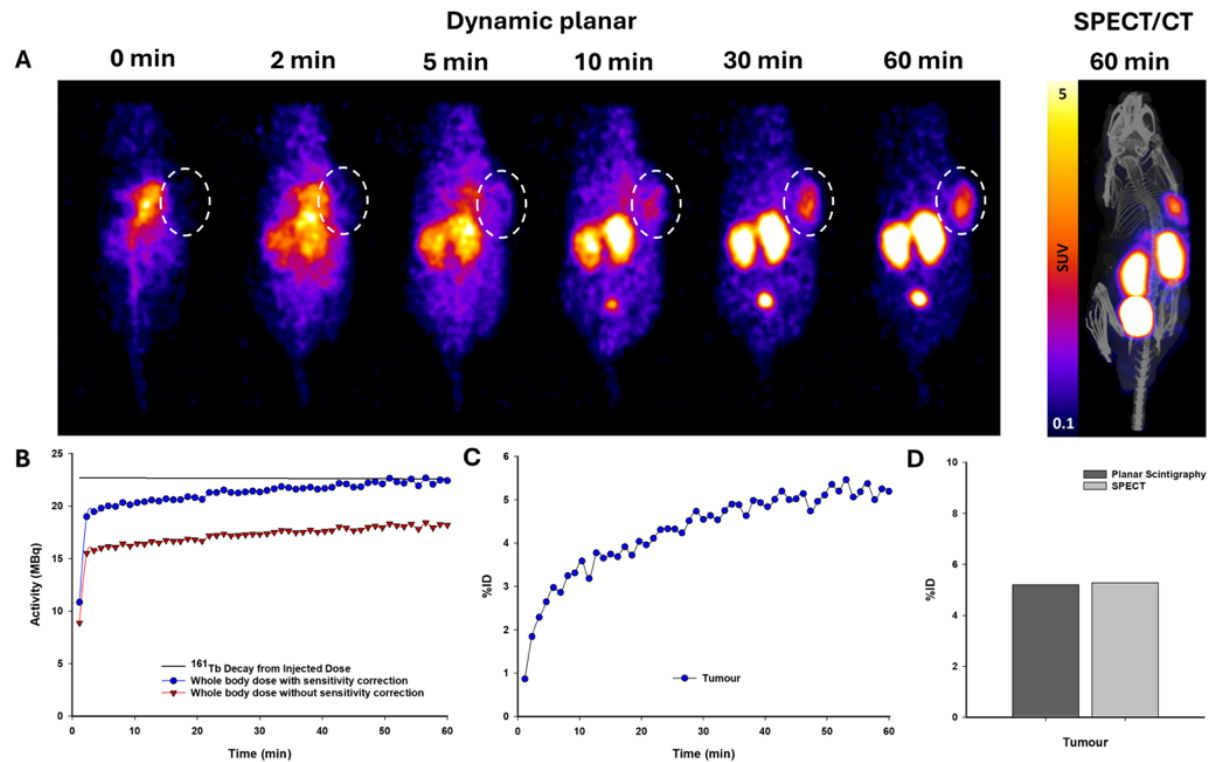


Figure 1. Tumour uptake as determined by planar scintigraphy and by SPECT/CT imaging, respectively

KEYNOTE LECTURE – O 13

Theranostic Radiopharmaceuticals: Lost in Translation?

M Schottelius

Laboratoire Translationnel des Sciences Radiopharmaceutiques, Service de médecine nucléaire et imagerie moléculaire, Département d'oncologie, Centre Hospitalier Universitaire Vaudois (CHUV), Agora, Bureau B25A/03/094, Rue du Bugnon 25A, CH-1011 Lausanne

Margret.Schottelius@chuv.ch

Over recent decades, a range of powerful theranostic concepts have successfully transitioned from preclinical research to clinical application, significantly advancing cancer diagnosis and treatment. Key targets such as somatostatin receptor subtype 2 (sst2), prostate-specific membrane antigen (PSMA), C-X-C chemokine receptor type 4 (CXCR4), and fibroblast activation protein (FAP) have served as benchmarks for this translational progress. This presentation aims to address two fundamental questions: What factors contributed to the successful clinical translation of these theranostic agents? And, crucially, what are the next steps required at the preclinical level to facilitate the clinical translation of new theranostic concepts? The discussion will explore current strategies aimed at enhancing the efficacy and performance of existing theranostic tracers, including optimization of pharmacokinetics and targeting specificity. Additionally, emerging theranostic targets that are currently under investigation will be presented, highlighting novel approaches in preclinical research that hold the potential to expand the range of cancers treatable through theranostics.

Professor Margret Schottelius – Biography



Margret Schottelius began her academic journey studying Chemistry at the University of Konstanz in Germany, completing her Bachelor's degree between 1992 and 1994. She then received a full sponsorship to study at Rutgers University in New Jersey, USA, from 1994 to 1995. She continued at ETH Zurich, where she earned her Master's degree in Chemistry in 1997, conducting research for her Master's thesis at the Laboratoire de Pharmacochimie Moléculaire of Université Louis Pasteur in Strasbourg, France (1997-1998). In 2002, she obtained her Ph.D. in Radiopharmaceutical Chemistry at TU Munich, Germany, under Prof. Dr. Hans-Jürgen Wester.

Following a postdoctoral fellowship in the same group, Margret attained her habilitation in Nuclear Medicine and Radiopharmacy, earning the title of Private Dozent, in 2009. From 2010 to 2019, she was a Senior Research Associate at the Chair of Pharmaceutical Radiochemistry at TU Munich, led by Prof. Hans-Jürgen Wester, and was appointed Titular Professor at the Faculty of Medicine in 2017.

In 2019, she became Associate Professor for Radiopharmaceutical Sciences at CHUV and the University of Lausanne (UNIL) in Switzerland, where she now leads the Translational Radiopharmaceutical Sciences Lab at the Agora research centre. Her research focuses on developing and translating peptide-based radiopharmaceuticals for theranostic applications in oncology, with a strong focus on the tumour immune microenvironment since her move to Lausanne.



MR SOLUTIONS GROUP



MRS*DRYMAG

Preclinical MR scanner
Dry Magnet Technology

9.4T - 7.0T - 4.7T - 3.0T
Cryogen-free - large bore 42 cm

0011100001101001000001101101000

MRS*SPECT-PET/MR

Preclinical SPECT-PET/MR scanner
PET INSERT & SPECT CLIP-ON



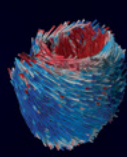
0000000001

000000000110010101001000010100010



MRS*SPECT-PET/CT

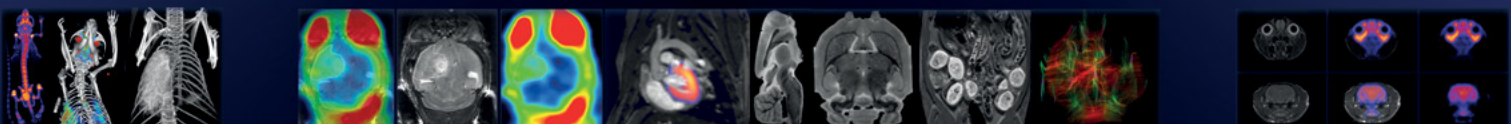
Preclinical SPECT-PET/CT scanner
CLIP ON Technology MR compatible

Oncology Angiography

Cardiology Diffusion

Neurology Relaxometry



MR SOLUTIONS GROUP
Imaging INNOVATION

MR SOLUTIONS GROUP
Ashbourne House, The Guildway,
Old Portsmouth Rd. Guildford,
Surrey, GU3 1LR
United Kingdom

information@mrsolutions.com
+44 (0)1483 906305
www.mrsolutions.com

P 01

CageTag: Co^{III}₄L₆ Tetrahedral Supramolecular Cages as a Universal Platform for Radiopharmaceutical DevelopmentI Renard^{1,2,*}, JD Wright^{1,2}, E Foyle³, I Middleton³, DP Roberts¹, PJ Lusby³, SJ Archibald^{1,2}¹Centre for Biomedicine and PET Research Centre, Hull York Medical School, University of Hull, Hull, UK; ²School of Biomedical Engineering and Imaging Sciences, King's College London, London, UK; ³EaStCHEM School of Chemistry, University of Edinburgh, Edinburgh, Scotland

* isaline.renard@kcl.ac.uk

The use of radiopharmaceuticals for imaging and therapeutic applications in cancer is generating a lot of interest, as evidenced by recent acquisitions of theranostic pairs by big pharmaceutical companies. However, the limited access to clinically-relevant radioisotopes, as well as the potentially challenging radiochemical synthesis, can hinder the development and wide-spread use of theranostics. The CageTag platform offers an attractive alternative to solve these issues. This strategy utilises self-assembling, kinetically inert Co^{III}₄L₆ tetrahedral cages that can be radiolabelled through non-covalent encapsulation of a radio-anion. This fast, reagentless and simple method could allow the development of “off-the-shelf” kits for virtually any radioisotope, offering more readily available theranostics in the clinic. Pilot experiments using SPECT/CT were previously reported showing a significant shift in biodistribution between free and encapsulated [^{99m}Tc]TcO₄⁻ [1].

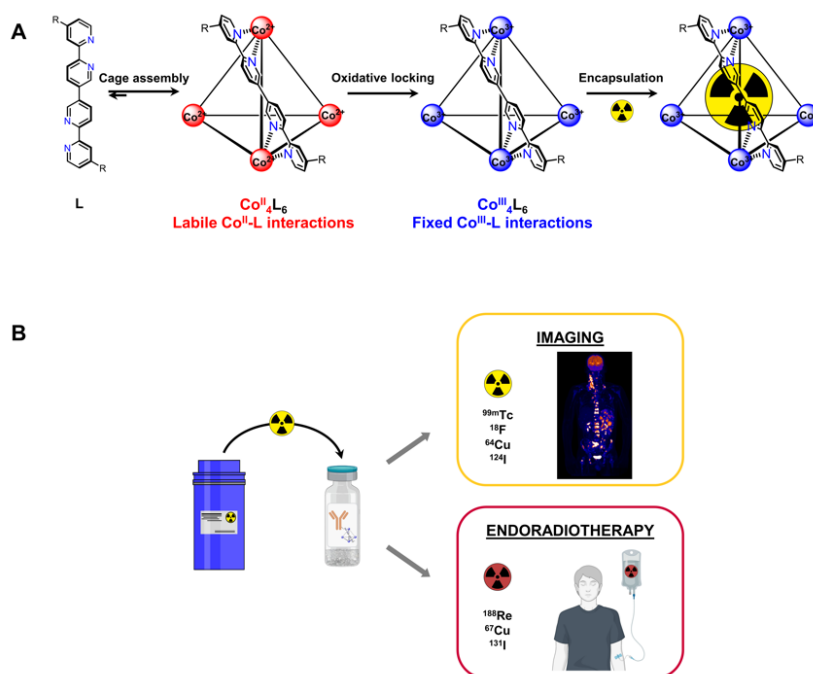


Figure 1. The CageTag strategy. (A) Schematic representation of the CageTag platform: self-assembly of the ligands L around Co^{II}, followed by oxidative locking of Co^{II} into Co^{III} to form a robust Co^{III}₄L₆ cage. The cage can be readily radiolabelled through non-covalent encapsulation of radio-anions such as [^{99m}Tc]TcO₄⁻. (B) The platform offers a reagentless, rapid and simple method for the preparation of radiopharmaceuticals that could allow the development of “off-the-shelf” kits for virtually all radioisotopes, facilitating “like-for-like” isotope switching and, thus, offering more readily available theranostics in the clinic.

Here, we expand our investigations to a library of cages, introducing different types of side-chain functionalisation of the ligand with varying chain length and polarity, in order to understand how these changes influence radiolabelling efficiency with $[^{99m}\text{Tc}]\text{TcO}_4^-$ along with the *in vitro* and *in vivo* properties of the resulting constructs. Dose-response experiments were carried out to determine the efficiency of $[^{99m}\text{Tc}]\text{TcO}_4^-$ encapsulation, followed by a range of *in vitro* stability assays in presence of competing anions (both “favourable guests” and physiologically-relevant anions). The radiolabelled cages were also evaluated in naïve animals by SPECT/CT, as well as by dynamic planar scintigraphy generating key dynamic information on the biodistribution of the radiolabelled constructs. Further experiments are currently ongoing to investigate the use of other radio-anions, the potential for targeting, as well as the development of non-equilibrium cages. Overall, the CageTag platform offers a novel reagentless, rapid and simple radiolabelling method, that represents an attractive alternative to a more traditional preparation of radiopharmaceuticals, with the potential to bring more readily available theranostics in the clinic.

[1] Burke, B. P. et al. *J. Am. Chem. Soc.* 2018, 140, 16877

P 02

New, Optimised Diphosphine Chelator Platforms for Receptor-targeted Tc-99m and Re-188 Radiopharmaceuticals

RE Nuttall*, IN Hungnes, TT Pham, OWL Carter, A Rigby, N Patel, Z Yu, J Cleaver, JD Young, J Sosabowski, PG Pringle, MT Ma

School of Biomedical Engineering & Imaging Sciences, King's College London, UK; Centre for Cancer Biomarkers and Biotherapeutics, Barts Cancer Institute, Queen Mary University of London, John Vane Science Centre, Charterhouse Square, London, EC1M 6BQ, UK; School of Chemistry, University of Bristol, UK

* rachel.nuttall@kcl.ac.uk

A challenge in molecular imaging with radiometals is designing chelators that radiolabel under simple, rapid, and physiologically compatible protocols. Phosphine chelators bind ^{99m}Tc in quantitative RCYs under mild conditions. We have previously shown that anhydride-derived diphosphines provide an adaptable chelator platform for development of targeted ^{99m}Tc and ^{188}Re radiopharmaceuticals [1–3]. Our aim was to optimise this diphosphine technology to enable quantitative RCYs ($\geq 95\%$) with ^{99m}Tc .

Here we show two novel diphosphines, DPAn and DPEG, can be reacted with a wide range of biological targeting vectors. Exemplar diphosphine-peptide conjugates, DPAn-PSMA and DPEG-PSMA, can be radiolabelled with ^{99m}Tc , using a one-step, kit-based procedure to form $[^{99m}\text{Tc}][\text{TcO}_2(\text{DPX-PSMA})_2]^+$ ($X = \text{An, EG}$) complexes in $\geq 95\%$ RCYs. Radiolabelling with ^{188}Re was achieved using a two-step, kit-based procedure to form $[^{188}\text{Re}][\text{ReO}_2(\text{DPX-PSMA})_2]^+$ complexes both in approx. 60% RCY. These radiochemical yields are a marked improvement from first-generation diphosphine radiotracers. The new DPX-PSMA conjugates can also radiolabel $^{64}\text{Cu}^+$, to form $[^{64}\text{Cu}][\text{Cu}(\text{DPX-PSMA})_2]^+$, enabling molecular PET imaging with this platform.

Biodistribution studies of $[^{99m}\text{Tc}][\text{TcO}_2(\text{DPX-PSMA})_2]^+$ ($X = \text{An, EG}$) in mice bearing PSMA-positive tumours (DU145-PSMA and LNCaP) showed accumulation in tumours (2–5 %ID/g) and spleen for both tracers, with low non-target uptake.

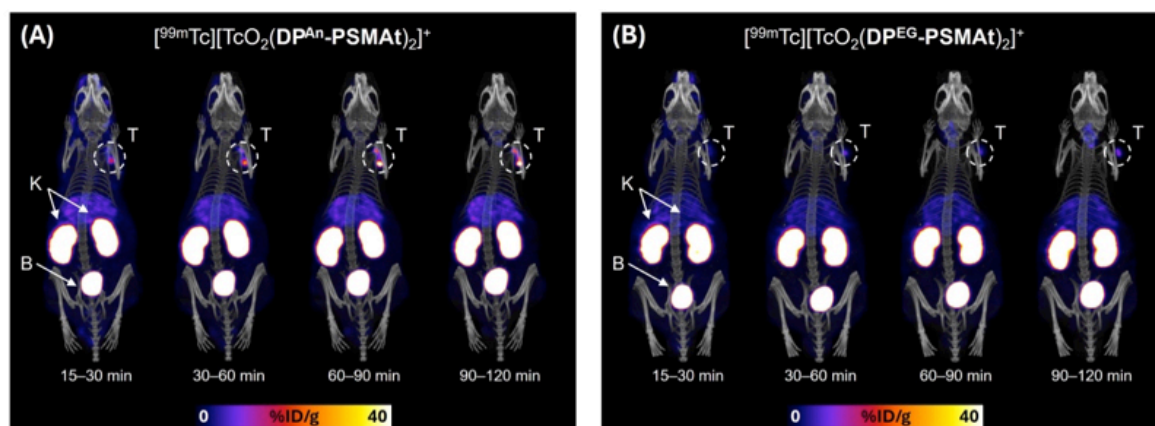


Figure 1. Whole body SPECT/CT maximum intensity projections of SCID/Beige mice bearing DU145-PSMA tumours administered either $[^{99m}\text{TcO}_2(\text{DPAn_PSMA})_2]^+$ (A) or $[^{99m}\text{TcO}_2(\text{DPEG_PSMA})_2]^+$ (B), from 15 min to 2 h post-injection. T = tumour, K = kidneys, B = bladder.

SPECT/CT images of mice indicated that DU145-PSMA tumours could be clearly delineated, with fast clearance from circulation and renal excretion, consistent with biodistribution data. Analysis of excreted urine showed that both tracers were excreted intact, indicating high stability under physiological environments. By tuning the diphosphine chelator, ^{99m}Tc radiolabelling RCYs improved to $\geq 95\%$ for these diphosphine-conjugates using a simple, rapid, translatable radiolabelling process. Combined with existing infrastructure, this platform could provide increased patient access to the benefits of receptor-targeted molecular SPECT imaging.

- [1] Hungnes, I. N.; Al-Saleme, F.; Gawne, P. J.; Eykyn, T.; Atkinson, R. A.; Terry, S. Y. A.; Clarke, F.; Blower, P. J.; Pringle, P. G.; Ma, M. T. One-Step, Kit-Based Radiopharmaceuticals for Molecular SPECT Imaging: A Versatile Diphosphine Chelator for ^{99m}Tc Radiolabelling of Peptides. *Dalton Trans.* 2021, 50 (44), 16156–16165.
- [2] Hungnes, I. N.; Pham, T. T.; Rivas, C.; Jarvis, J. A.; Nuttall, R. E.; Cooper, S. M.; Young, J. D.; Blower, P. J.; Pringle, P. G.; Ma, M. T. Versatile Diphosphine Chelators for Radiolabeling Peptides with ^{99m}Tc and ^{64}Cu . *Inorg. Chem.* 2023, 62 (50), 20608–20620.
- [3] Pham, T. T.; Hungnes, I. N.; Rivas, C.; Cleaver, J.; Firth, G.; Blower, P. J.; Sosabowski, J.; Cook, G. J. R.; Livieratos, L.; Young, J. D.; Pringle, P. G.; Ma, M. T. Receptor-Targeted Peptide Conjugates Based on Diphosphines Enable Preparation of ^{99m}Tc and ^{188}Re Theranostic Agents for Prostate Cancer. *J. Nucl. Med.* 2024, 65 (7), 1087–1094.

P 03

Dithiocarbamates for Molecular Imaging with Technetium-99m Labelled Peptides

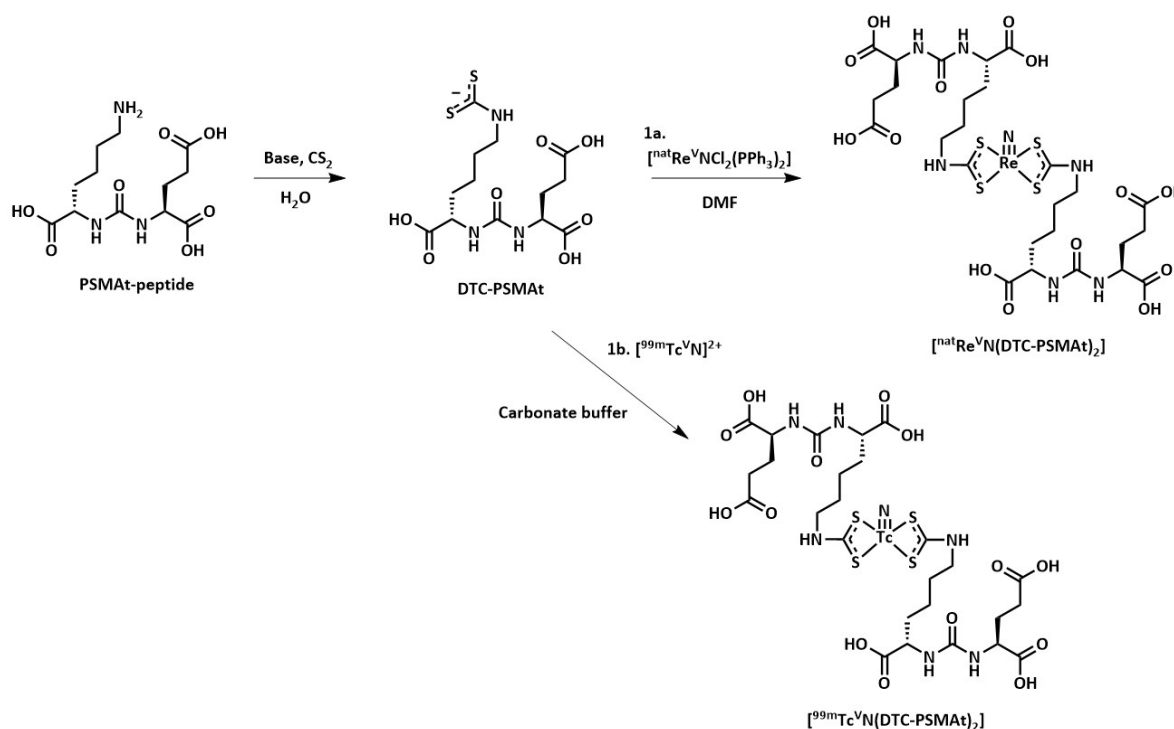
JS Shin, RE Nuttall, OWL Carter, RTM Rosales, G Hogarth, MT Ma

School of Biomedical Engineering & Imaging Sciences, King's College London, UK

k21141670@kcl.ac.uk

The radionuclide Tc-99m ($t_{1/2} = 6\text{h}$, 89% abundance, $E_{\gamma} = 141\text{ keV}$) is a gamma-emitter used in radiotracers for diagnostic SPECT (Single Photon Emission Computed Tomography) and/or gamma-scintigraphy imaging. $^{99\text{m}}\text{Tc}$ -labelled radiopharmaceuticals are produced using kits, however most Tc-99m radiotracers are perfusion imaging agents. New efficient Tc-99m chelators are required to enable incorporation of Tc-99m into a targeting biomolecule, for receptor-targeted molecular SPECT/gamma-scintigraphy imaging. Dithiocarbamate (DTC) chelators are attractive candidates for this purpose, as they are highly adaptable and versatile in their binding to a wide range of oxidation states of metals.

This project aims to develop a DTC derivative of the prostate-specific membrane antigen targeted (PSMA) peptide, for Tc-99m radiolabelling and SPECT molecular imaging of prostate cancer. The chemistry of rhenium (Re) and Tc are closely similar. A DTC was prepared from a primary amine derivative of the PSMA-peptide, to yield DTC-PSMA (Figure 1). The non-radioactive Re and radioactive Tc-99m complexes were prepared, with the latter synthesised in high radiochemical yield (>95%). The $^{99\text{m}}\text{Tc}$ complex showed high stability in serum (>80%) and *in vitro* studies are currently underway.

**Figure 1.** Synthetic route to DTC-PSMA

P 04

New Hybrid Hydroxypyridinone-aza-crown-macrocylic Chelators for Molecular Imaging and Radiotherapy

RAJ Kenrick*, A Rigby, RE Nuttall, TT Pham, C Rivas, SM Cooper, OWL Carter, T Hicks, NJ Long, MT Ma

King's College London; Imperial College London

* rory.kenrick@kcl.ac.uk

Macrocyclic chelators incorporating aza-18-crown-6 rings have shown promise for stable encapsulation of f-block metal ions, notably radionuclides of Tb^{3+} , Lu^{3+} , Ac^{3+} and Th^{4+} [1,2]. Multidentate ligands incorporating hydroxypyridinone (HOPO) motifs have demonstrated versatility in complexation of many radionuclides, including $[^{68}Ga]Ga^{3+}$ and $[^{227}Th]Th^{4+}$ [3,4]. Given this previous success, with notable affinity of both families toward electronically ‘hard’ metal ions, three novel hybrid chelators, 2C/3C-DIHOPO and 3C-TRIIHOPO (**Figure 1a**) have been synthesised. Each contains an aza-18-crown-6 crown ether macrocycle functionalised with pendent 3,2-HOPO groups for additional coordination of metal ions.

The ability of 2C/3C-DIHOPO to coordinate La^{3+} (as a surrogate of Ac^{3+}), Tb^{3+} , Lu^{3+} and $[^{232}Th]Th^{4+}$ has been studied. Results suggest that while 3C-DIHOPO chelates all investigated f-block ions effectively, 2C-DIHOPO is most effective with smaller ions in the series (Tb^{3+} and Lu^{3+}). Furthermore, radiolabelling studies with radiotherapeutic, β^- -emitting $[^{161}Tb]Tb^{3+}$ (β^- , $t_{1/2} = 6.9$ d) indicate all ligands bind the radiometal.

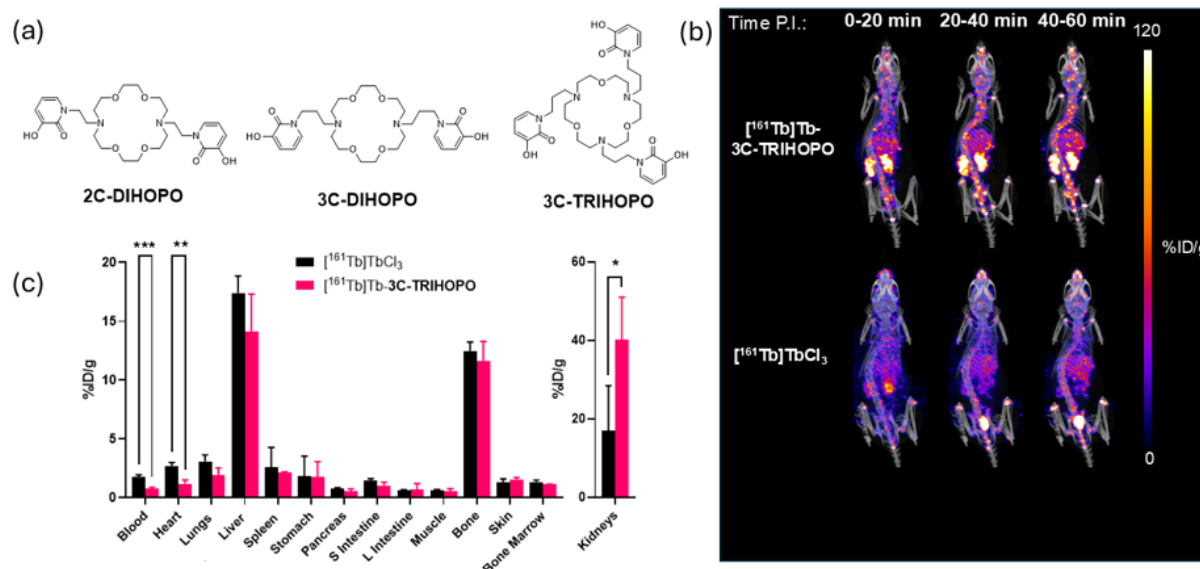


Figure 1. (a) ChemDraw structures of chelators discussed in this work. (b) SPECT-CT images of healthy mice taken in 20-minute intervals up to 1h post-injection (P.I.) of both $[^{161}Tb]Tb$ -3C-TRIIHOPO (top) and $[^{161}Tb]TbCl_3$ (bottom), showing the percentage injected dose per gram (%ID/g) of tissue in each case. Colour bar given for reference. (b) Ex-vivo biodistribution of healthy mice n=4 per condition) 1h post- injection with $[^{161}Tb]TbCl_3$ (black bars) and $[^{161}Tb]Tb$ -3C-TRIIHOPO (pink bars), with error bars provided for each organ. Key: ***p=0.000715, **p=0.00294 and *p=0.0442.

Out of these three new radiolabelled chelators, [^{161}Tb]Tb-3C-TRIOPO was prepared in highest radiochemical yield. Therefore, the stability of [^{161}Tb]Tb-3C-TRIOPO was then studied by incubating the radiolabelled complex in human serum at 37 °C, indicating the complex was 66% and 23% intact after 1 h and 24 h, respectively. The Tb-labelled complex was also studied *in vivo* by SPECT-CT imaging up to 1 h post-injection, and by obtainment of an ex-vivo biodistribution profile. These data are consistent with serum studies, suggesting initial stability of the radiolabelled complex, but with complex dissociation over time (**Figure 1b/c**). These findings explore the potential of 3C-TRIOPO as a novel ligand for Tb-161-based chelation and therapy.

- [1] A. Hu et al., *Inorg. Chem.*, 2022, 61, 12847-12855.
- [2] N. A. Thiele et al., *Angew. Chem., Int. Ed.*, 2017, 56, 14712-14717.
- [3] T. Ramdahl et al., *Bioorg. Med. Chem. Lett.*, 2016, 26, 4318-4321.
- [4] J. D. Young et al., *J. Nucl. Med.*, 2017, 58, 1270-1277.

P 05**Functional ^{18}F -FDG PET in the Rat Brain: Inter-animal Variability and Normalization Strategies**

C Hery*, F Hontonnou, A Tourais, M Guillermier, M Benfissa, O Barret, N van Camp, C Baligand

Université Paris-Saclay, Commissariat à l'Energie Atomique et aux Energies Alternatives (CEA), Centre National de la Recherche Scientifique (CNRS), Molecular Imaging Research Center (MIRCent), Laboratoire des Maladies Neurodégénératives, 92260 Fontenay aux Roses, France

* cameron.hery@cea.fr

Measuring sensory-stimulus evoked changes in glucose metabolism in rodents using ^{18}F -FDG PET is challenging, partly due to the numerous physiological factors affecting FDG uptake and quantification [1,2]. Here, we report on our current effort towards functional ^{18}F -FDG PET in rats. We performed ^{18}F -FDG PET scans (60 min acquisitions) under various sensory stimulation conditions in female rats anesthetized with medetomidine, including visual (n=9), whiskers (n=6), and paw electrical stimulation (n=6). In the visual stimulation group, two separate scans were conducted within 10 days for each animal, either during exposure to a 2Hz-flashing light or without light (control), in a randomized order. Dynamic PET images were corrected for decay, scatter and attenuation during reconstruction; and all data sets were processed in Pmod3.8. SUV images (normalized to dose and body weight) were registered to the SIGMA atlas. For regional FDG uptake comparisons, the last 30 min of acquisition were averaged. We explored different normalization strategies and analysed their impact on effect-size in our sample (Cohen's D for repeated measures, drm). In the visual stimulation group, we saw that the drm of the $\text{SUV}_{\text{colliculus}}$ ($\text{drm}_{\text{colliculus}}=0.07$) remained very low when data were normalized to the Pons ($\text{drm}_{\text{colliculus}/\text{Pons}}=0.11$), but increased when normalizing to full brain ($\text{drm}_{\text{colliculus}/\text{Full Brain}}=0.53$) or lateral parietal associative cortex SUV ($\text{drm}_{\text{colliculus}/\text{LPAC}}=0.68$). However, these values remained below 0.8, which is considered a medium effect-size, making it difficult to draw definitive conclusion at this stage regarding the possible increase in $\text{SUV}_{\text{colliculus}/\text{LPAC}}$ seen in our data ($4.2 \pm 6.8\%$). Work is still underway to increase sample size in the paw and whisker stimulation groups, evaluate the effect of anesthesia on the results, and improve our post-processing and analysis approach.

[1] Proesmans, S. et al. Voxel-Based Analysis of [^{18}F]-FDG Brain PET in Rats Using Data-Driven Normalization. *Front Med (Lausanne)* 8, 744157 (2021).

[2] Miranda, A., Bertoglio, D., Stroobants, S., Staelens, S. & Verhaeghe, J. Translation of Preclinical PET Imaging Findings: Challenges and Motion Correction to Overcome the Confounding Effect of Anesthetics. *Front Med (Lausanne)* 8, 753977 (2021).

P 06**A Roadmap for [¹¹C]BU99008 PET Imaging of Astrocyte Reactivity in Rodent Models**

J Jager, M Corbel, T Percerou, F Hontonnou, M Benfissa, C Jan, Y Bramoullé, O Barret, N van Camp

Université Paris-Saclay, Commissariat à l'Energie Atomique et aux Energies Alternatives (CEA), Centre National de la Recherche Scientifique (CNRS), Molecular Imaging Research Center (MIRCent), Laboratoire des Maladies Neurodégénératives

* nadja.van-camp@cea.fr

Imidazoline I-2 subtype receptors (I2-IR) are a heterogeneous family of proteins, expressed mainly by glial cells. [¹¹C]BU99008 is a highly specific PET ligand for I2-IR, and clinical studies in early AD patients have reported a higher PET signal compared to age-matched controls [1,2]. However, post-mortem studies evaluating the binding of [³H]BU99008 in AD brains, showed loss of a very high affinity and the appearance of a very low affinity site, which should rather be predictive of a lower PET signal in AD patients and thus contrary to the *in vivo* observations [3]. As drug treatment of I2-IR is a potential therapeutic strategy, it is important to understand potential changes of I2-IR with regards to changes in affinity for I2-IR ligands.

Our aim is, in a rodent model of astrocyte reactivity through localized viral-vector induced expression of CNTF, (1) to quantify the [¹¹C]BU99008 PET signal associated with astrocyte reactivity; (2) to evaluate in self-blocking studies the potential change in affinity of [¹¹C]BU99008 for the I2-IR in reactive astrocytes compared to non-reactive astrocytes.

We have successfully performed [¹¹C]BU99008 PET imaging in CNTF-induced (n=7) and WT (n=2) rats. As expected from the regional expression of I2-IR, the brain uptake of [¹¹C]BU99008 was highest in the striatum, hippocampus and thalamus. The PET signal was higher in the CNTF-induced region compared to the contralateral side (**Figure 1**). Self-blocking studies induced dose-dependent reduction of the PET signal in all brain regions. Analysis of the occupancy is ongoing to evaluate a potential change in affinity of [¹¹C]BU99008 for I2-IR in CNTF-reactive astrocytes compared to non-reactive astrocytes. Next, three-dimensional density maps derived from GFAP immunohistochemistry will be correlated with the PET signal. These results will provide a roadmap for I2-IR PET imaging in rodent models of neurodegenerative diseases as a tool to assess drug target engagement *in vivo*.

- [1] Calsolaro V, Matthews PM, Donat CK, Livingston NR, Femminella GD, Guedes SS, et al. Astrocyte reactivity with late-onset cognitive impairment assessed *in vivo* using (11)C-BU99008 PET and its relationship with amyloid load. *Molecular psychiatry*. 2021;26(10):5848-55.
- [2] Livingston NR, Calsolaro V, Hinz R, Nowell J, Raza S, Gentleman S, et al. Relationship between astrocyte reactivity, using novel (11)C-BU99008 PET, and glucose metabolism, grey matter volume and amyloid load in cognitively impaired individuals. *Molecular psychiatry*. 2022.
- [3] Kumar A, Koistinen NA, Malarte ML, Nennesmo I, Ingelsson M, Ghetti B, et al. Astroglial tracer BU99008 detects multiple binding sites in Alzheimer's disease brain. *Molecular psychiatry*. 2021;26(10):5833-47.

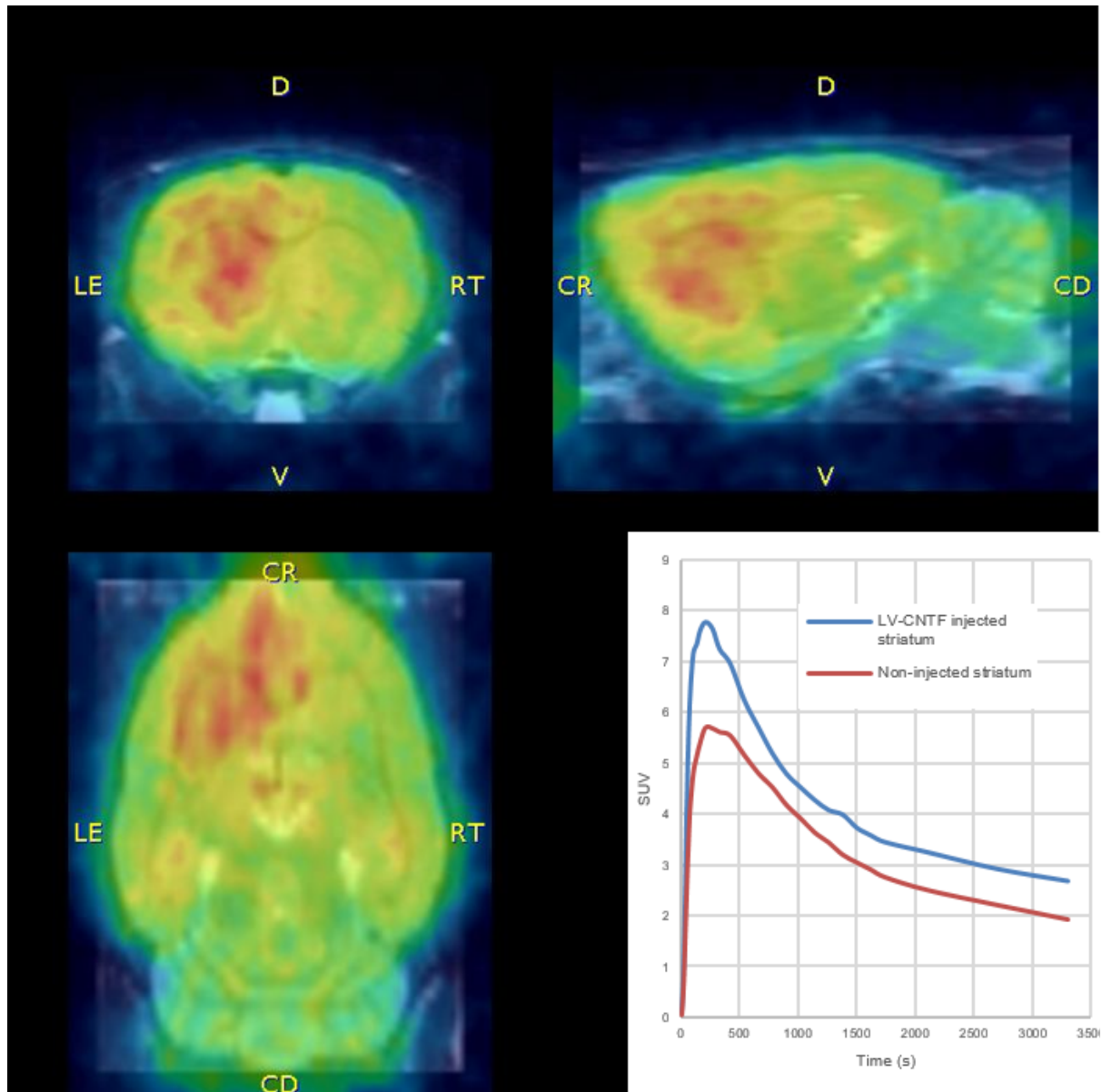


Figure 1. [¹¹C]BU99008 PET imaging in CNTF-induced rats and controls

P 07**PET/CT Imaging of Blood-Brain Barrier Integrity and Inflammatory Tracers during Alzheimer's Disease**

BM Alenezi, SJ Paisey, TR Hughes

Cardiff University

* AleneziBM@cardiff.ac.uk

Alzheimer's Disease (AD) is the most common cause of dementia in elderly people. Although the exact pathogenesis of AD remains unclear, recent research implicates the immune complement system in the progression of the disease. Immuno-PET is an imaging technique used to improve the visualization of a target site by combining the high sensitivity of PET with the specificity of monoclonal antibodies (mAbs). BB5.1 is a monoclonal antibody targeted against the immune complement protein C5. Previous results have shown that feeding 3xTG AD mice a high fat diet (HFD) worsens the inflammatory state in this model, has a negative impact on cognition and causes neuronal spine density to decrease and that these effects were counteracted by supplementation of the HFD with probiotics. Our hypothesis is that Alzheimer's neurodegeneration will enable the systemically circulating radioactive labelled BB5.1 to cross BBB and detect complement activity in the diseased brain of AD mice models.

To test our hypothesis, we have performed *in vivo* imaging of mice 3xTG AD using Zr-89 labelled BB5.1 antibody to assess its biodistribution and brain penetrance and F-18 FDG to assess brain metabolism. Mice were subjected to 2 blocks of imaging one at baseline (6 months) and one at end point (9 months), each imaging block consisted of injection of 2MBq of ⁸⁹Zr-labeled DFO-BB5.1 or negative control antibody ⁸⁹Zr-DFO-D1.3 followed by PET/CT imaging 24h, 72h, and 144h. Mice were also scanned at 192h with F-18 FDG (10MBq). After the baseline scans mice were split into 4 groups and received either HFD + probiotic, HFD, normal chow + probiotic or normal chow for 3 months. Mice were also assessed for novel object recognition at baseline and at end point. Further techniques, such as immunohistochemistry and qPCR, will be used to confirm the presence of inflammation and disease in these animals and the integrity of the BBB.

In vitro haemolysis assays confirmed biological activity of the radiolabelled BB5.1 and all PET/CT scans and behavioural tests have been successfully completed. Analysis of the data is underway and will be completed by the time of the conference.

It is hoped these preliminary experiments will pave the way to use ⁸⁹Zr-DFO-BB5.1 in PET/CT imaging to examine BB5.1 biodistribution in Alzheimer's disease models as a potential marker of BBB breakdown during neurodegeneration in AD.

- [1] Hong, S. et al. 2016. Science 352(6286), pp. 712-716.
- [2] Huugen, D. et al. 2007. Kidney International 71(7), pp. 646-654.
- [3] Webberley, T. S. et al. 2023. International Journal of Molecular Sciences 24(5).
- [4] Wyss-Coray, T. and Rogers, J. 2012. Cold Spring Harbor Perspectives in Medicine 2(1), p. a006346.
- [5] Zelek, W. M., Menzies, G. E., Brancale, A., Stockinger, B. and Morgan, B. P. 2020. Immunology 161(2), pp. 103-113.

P 08

Preclinical Animal Imaging of ALL-in-1, Multimodal, Multitargeted Radiotheranostic Agents by PET/OI towards combined PDT/PET

C Sathiyajith, F Habte, NEQ Callab, N Malik, A Garofalakis, J Tchicaya

SAAINNOVATE, Stanford University(SCi3), BioSapce Lab

* sjithcw@gmail.com

Development of PET/MRI/OI radiotheranostic agent based on EDTA bisamide ligand with a pyridine-based fluorophore. Multitargeted anticancer activity for TSPO and a kinase(s), supported by its affinity for HSA, facilitating therapy and monitoring for Melanoma by hybrid PET/OI agent.

^{64}Cu radiolabelling of L1 in NaOAc & MES buffers was completed within 30 min. (pH 6, 40 °C), purified by HPLC. RCY was evaluated by iTLC. Xenografts were generated by injecting B16-F10 cells (10⁵) subcutaneously into the shaved lateral flank of C57BL/6J mice. All mice received an average dose of ~190uCi ^{64}Cu radiolabeled tracer via I.V. injection. Two groups of WT mice underwent dynamic/static scans by Sofie PET/CT and Bruker PET/MRI (7T) at 1h and 24 h time points with 10 min 20 min acquisition respectively. Imaging of control mice injected with $^{64}\text{CuCl}_2$ +saline was performed for comparison. Both ex vivo biodistribution and Image-based quantification were done. Docking studies with TSPO, FAP, and EGFR kinases were conducted by AUTODOCK Vina and validated by MD simulation via My Presto®. *In vitro* optical properties evaluated by phantoms.

iTLC indicated strong radiolabelling (> 96 % in MES and >95 % in NaOAc). Very high tumor uptake (11.6 % ID/g over 24 h) from PET/MRI validated by PET/CT and exvivo biodistribution studies, Docking revealed inhibition of TSPO, FAP (allosteric), and EGFR (-6.9, -7.0 and 6.7 Kcal/mol), validated by their respective co-crystallized ligands and commercial standards and by MD simulation. Excitation-emission optimized; 462 nm and 597 nm (DMSO/H₂O).

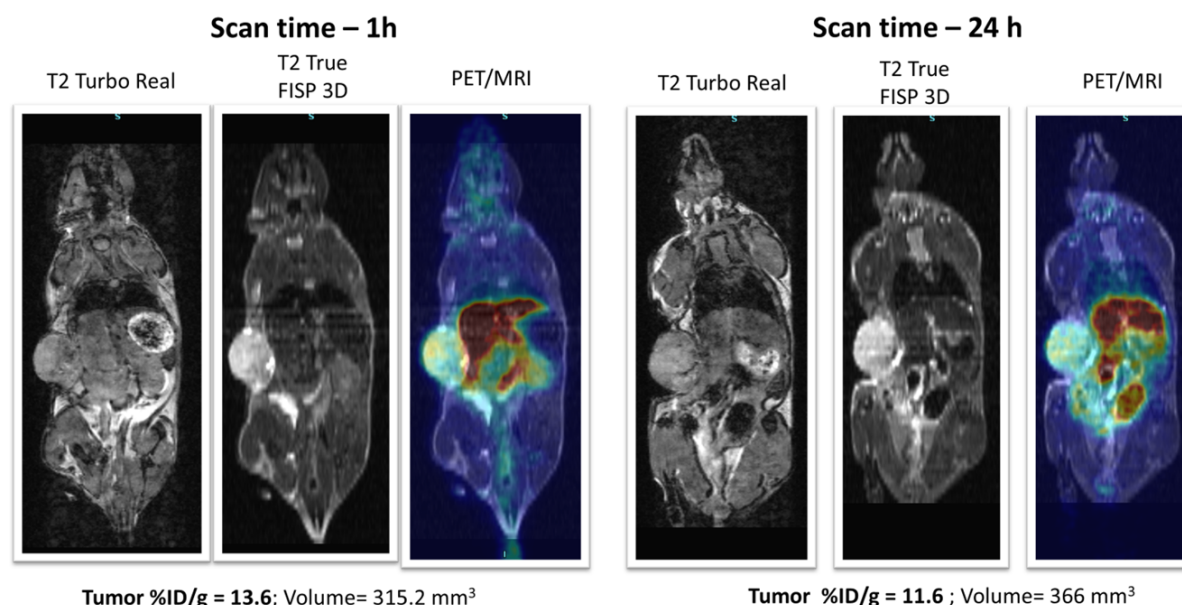


Figure 1. Comparison of tumour uptake by PET/MRI of ^{64}Cu -L1 – sagittal view

Very high tumor uptake (11.6% ID/g over 24h) justified diagnostic efficacy by both PET/MRI and PET/CT imaging with demarcated tumor margins. The translational capacity of ^{64}Cu -L1 as a PET/OI agent is well established. Potential coupling with $\text{Re}(\text{CO})_3\text{Cl}$ will aid in novel PDT/PET theranostics. SWIR Fluorescence lifetime imaging application is exploited at present.

- [1] C. Sathiyajith, A. J. Hallett and P. G. Edwards, Synthesis, photophysical characterization, relaxometric studies and molecular docking studies of gadolinium-free contrast agents for dual modal imaging, *Results Chem.*, 4, 100307, (2022).

P 09

Novel Dual CXCR4- and ACKR3-targeted Theranostic Agents for PET/SPECT Imaging and Therapeutic Applications in Cancer

J Wood^{1,*}, I Renard^{1,2}, JD Wright^{1,2}, J Domarkas², BP Burke², D Schols³, T D'Huys³, T Van Loy³, TJ Hubin⁴, SJ Archibald^{1,2}

¹Department of Imaging Chemistry and Biology, King's College London, SE1 7EH, London, UK;

²Department of Chemistry and Positron Emission Tomography Research Centre, University of Hull, HU6 7RX, Hull, UK; ³Rega Institute for Medical Research, KU Leuven, 3000 Leuven, Belgium;

⁴Department of Chemistry and Physics, Southwestern Oklahoma State University, OK 73096, USA

* james.g.wood@kcl.ac.uk

The chemokine receptors CXCR4 and ACKR3 (previously CXCR7) have been shown to be overexpressed in many different cancers [1] and usually indicate a poor prognosis [2]. Many imaging agents and therapeutic compounds have been studied for the targeting of CXCR4; however, few exist for ACKR3. Due to the collaborative nature of CXCR4 and ACKR3, targeting both receptors simultaneously could lead to improved therapeutic outcomes.

We have previously generated an extensive library of CXCR4-targeted configurationally-restricted tetraazamacrocycles, such as the high-affinity CXCR4 antagonist Cu₂CB-Bicyclam [3]. As these derivatives are amenable to radiolabelling with isotopes of copper (⁶⁴Cu for PET and ⁶⁷Cu for SPECT and radionuclide therapy), we validated this approach in PET imaging studies, showing high and specific tumour uptake of the ⁶⁴Cu-radiolabelled analogue, [⁶⁴Cu]CuCB-Bicyclam, in mice implanted with U87-CXCR4 xenografts [4].

We recently identified a subgroup with high affinity for both CXCR4 and ACKR3, with IC₅₀ values as low as 0.9 nM and 40 nM for CXCR4 and ACKR3, respectively. Here, we report on the *in vitro* evaluation of these new CXCR4/ACKR3 dual binding agents, along with ⁶⁷Cu-radiolabelling of lead candidates and subsequent *in vivo* evaluation in mice implanted with CXCR4- and ACKR3-overexpressing xenografts, showing high tumour uptake. CXCR4-specificity was confirmed in blocking studies using the high-affinity CXCR4 antagonist, Cu₂CB-Bicyclam (Figure 1). Future work will focus on confirming specificity of the novel dual inhibitors for ACKR3 *in vivo* and gaining a better understanding of the interactions between these derivatives and the two chemokine receptors of interest. Further evaluation will be carried out in a range of tumour models with different expression levels of CXCR4 and ACKR3, as well as in radiopharmaceutical therapy experiments.

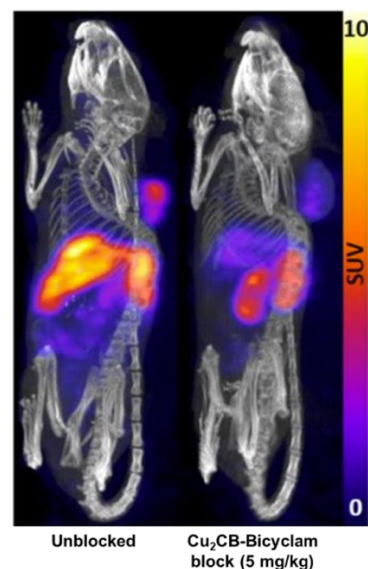


Figure 1. Representative 30 min SPECT/CT scan of ⁶⁷Cu-radiolabelled CXCR4/ACKR3 dual inhibitor in U87-CXCR4 tumour-bearing mice, unblocked (left) and blocked with 5 mg.kg (i.p.) of Cu₂CB-Bicyclam (right), imaged at 3 d post-injection.

- [1] Wani, N.; Nasser, M. W.; Ahirwar, D. K.; Zhao, H.; Miao, Z.; Shilo, K.; Ganju, R. K. C-X-C motif chemokine 12/C-X-C chemokine receptor type 7 signaling regulates breast cancer growth and metastasis by modulating the tumor microenvironment. *Breast Cancer Res* 2014, 16 (3), R54.
- [2] Zlotnik, A.; Burkhardt, A. M.; Homey, B. Homeostatic chemokine receptors and organ-specific metastasis. *Nat Rev Immunol* 2011, 11 (9), 597-606.
- [3] Khan, A.; Nicholson, G.; Greenman, J.; Madden, L.; McRobbie, G.; Pannecouque, C.; De Clercq, E.; Ullom, R.; Maples, D. L.; Maples, R. D.; et al. Binding optimization through coordination chemistry: CXCR4 chemokine receptor antagonists from ultrarigid metal complexes. *J Am Chem Soc* 2009, 131 (10), 3416-3417.
- [4] Burke, B. P.; Miranda, C. S.; Lee, R. E.; Renard, I.; Nigam, S.; Clemente, G. S.; D'Huys, T.; Ruest, T.; Domarkas, J.; Thompson, J. A.; et al. (64)Cu PET Imaging of the CXCR4 Chemokine Receptor Using a Cross-Bridged Cyclam Bis-Tetraazamacrocyclic Antagonist. *J Nucl Med* 2020, 61 (1), 123-128.

P 10

Imaging Redox and Hypoxia in Metastatic Non-small Cell Lung Cancer

JL Bowden, SM Harding, SN Dos Santos, GO Fruhwirth, TH Witney*

King's College London

* tim.witney@kcl.ac.uk

Metastasis is the leading cause of death in patients with cancer [1]. In lung cancer, metastatic disease is present in over 50% of patients at diagnosis, resulting in a 5-year survival rate of just 8% [2]. Whilst increased antioxidant production is found in metastases, its complex role in the metastatic cascade is poorly understood [3-5].

To investigate the role of redox regulation and hypoxia in metastatic lung cancer, the metastatic lung cancer murine cell line, CMT167, was genetically engineered through lentiviral transduction with a hypoxia-sensitive reporter system (Figure 1A). This hypoxia-sensitive reporter system contains fluorescent proteins (mCherry and GFP), the sodium iodide symporter (NIS), and Cre-ERT2, to enable *in vivo* fate-mapping and quantification of hypoxia exposure by SPECT imaging, following tamoxifen administration.

In vitro validation of the reporter cell line, through flow cytometry, fluorescence microscopy, and [^{99m}Tc]pertechnetate radiotracer uptake assays confirmed the correct expression, localisation, and function of the imaging reporters (Figure 1B-F). 85.3±4.3% hypoxia-sensitive ‘switching’ occurred following tamoxifen administration and exposure to 1% O₂ *in vitro* for 24h (Figure 1E). Next, CMT167 reporter cells, were grown in a subcutaneous, syngeneic murine model. The tumours maintained fluorescence *in vivo* and did not undergo hypoxia-sensitive ‘switching’ in the absence of tamoxifen. Tamoxifen-dependent hypoxia-sensitive NIS expression was confirmed by *in vivo* SPECT imaging with [^{99m}Tc]pertechnetate, resulting in an increase in tumour uptake from 2.2±0.7 to 7.9±1.7% ID/g (Figure 1G-H).

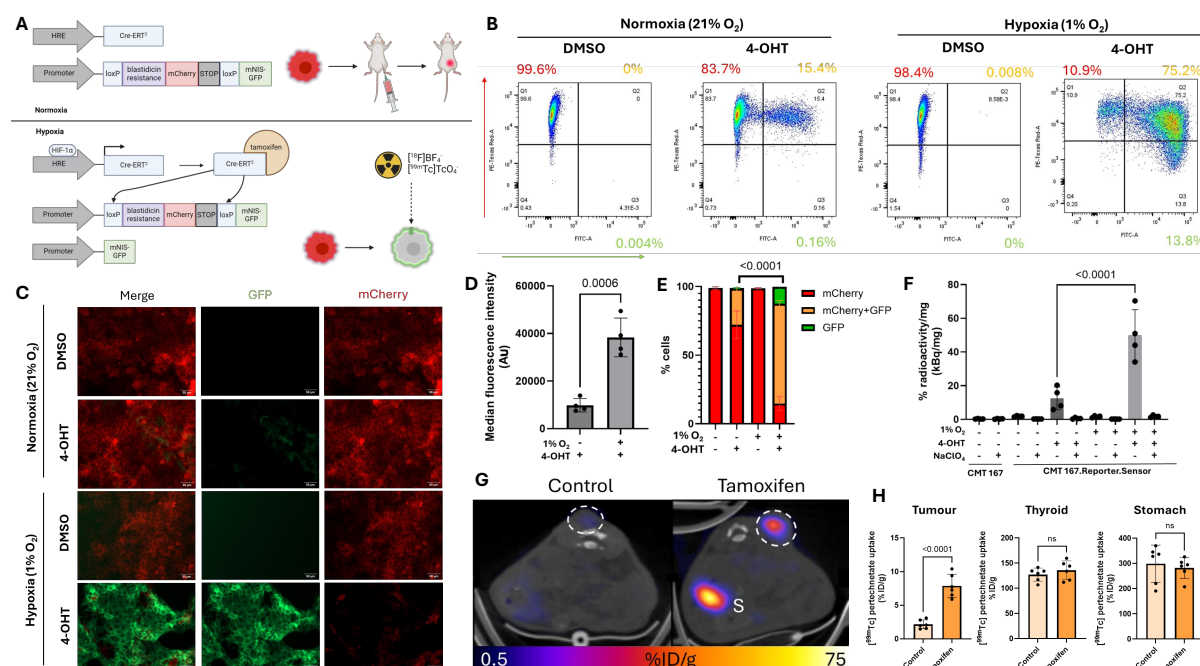


Figure 1. Characterisation of the engineered hypoxia-sensitive reporter system

Here, we demonstrate this hypoxia-sensitive reporter system functions both *in vitro* and *in vivo* in an immunocompetent murine model following tamoxifen administration. Next, the validated reporter cell line will be grown in an orthotopic murine model to better understand the link between hypoxia exposure and metastases. Combining this reporter system with [¹⁸F]FSPG PET imaging will further investigate whether exposure to hypoxia primes cancer cells to upregulate their antioxidant response to facilitate successful migration to distant sites.

- [1] <https://www.who.int/news-room/fact-sheets/detail/cancer>.
- [2] SEER*Explorer: An interactive website for SEER cancer statistics. Surveillance Research Program, N.C.I. Percent of Cases & 5-Year Relative Survival by Stage at Diagnosis: Lung and Bronchus Cancer, SEER 22 (Excluding IL/MA) 2013–2019. 2023
- [3] Tasdogan, A., J.M. Ubellacker, and S.J. Morrison, Redox Regulation in Cancer Cells during Metastasis. *Cancer Discov*, 2021. 11(11): p. 2682-2692.
- [4] Xing, F., et al., The Relationship of Redox With Hallmarks of Cancer: The Importance of Homeostasis and Context. *Front Oncol*, 2022. 12: p. 862743.
- [5] Acharya, A., et al., Redox regulation in cancer: a double-edged sword with therapeutic potential. *Oxid Med Cell Longev*, 2010. 3(1): p. 23-34.

Mediso Company profile 2024

Mediso is a leading supplier of molecular imaging techniques to the health care and medical research institutions of the world.

Mediso has a complete profile of system development, manufacturing, selling and servicing of multi-modality imaging devices. With over 30-years of expertise and 1,400+ clinical systems installed, Mediso offers complete solutions from imaging devices to evaluation and quantification software for both clinical patient care and scientific research.

Besides a unique triple modality clinical SPECT/CT/PET system, the new AnyScan® TRIO family is utilizing a triple head SPECT detector design and dedicated multi-pinhole collimation technology to achieve unparalleled sensitivity and quantitation accuracy especially for neuro- and cardiac imaging.

At EANM 2024 we proudly introduced the AnyScan® TRIO-TheraMAX SPECT/CT, the newest member of the family. With three wide energy-range detectors this system offers outstanding sensitivity and PET-like image quality for targeted alpha- and beta radionuclide therapy.

Mediso has a leader position in the preclinical nuclear imaging market with over 320 commissioned systems around the world. Beyond the market leading nanoScan® PET/CT and SPECT/CT, Mediso also offers standalone MRI and integrated PET/MRI systems based on a cryogen-free magnet with 3T or 7T field strength and a PET insert for simultaneous PET/MRI imaging.



Founded 1990 | Offices 7 | Employees 300+ | Publications 3200+ | Countries 100+



About us

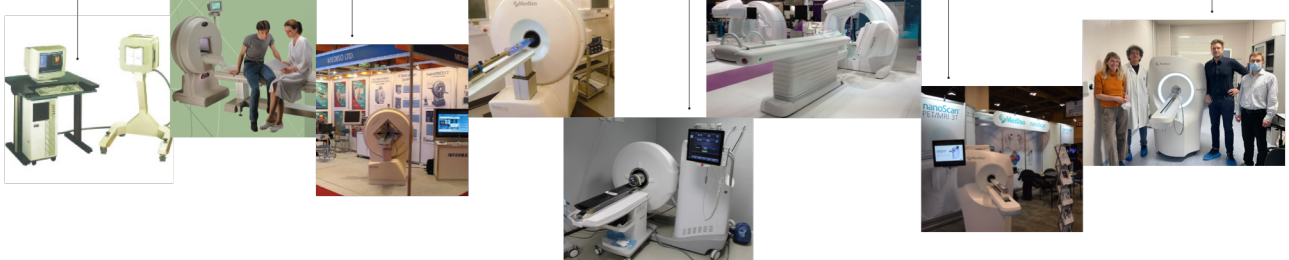
Mediso works in the field of **medical imaging** for **30+ years** with a profile of development, manufacturing, selling and servicing standalone and multi-modality imaging devices. The company offers complete solutions from hardware design to evaluation and quantification software for clinical patient care and preclinical research.

Preclinical systems 300+ | Clinical systems 1350+



Mediso has a leader position in the preclinical imaging market with **over 300 commissioned systems** around the world. Beyond the market leading nanoScan® PET/CT and SPECT/CT, Mediso also offers standalone MRI and integrated PET/MRI systems based on a cryogen-free magnet with 3T or 7T field strength and a PET insert for simultaneous PET/MRI imaging. Products are sold directly or through a distribution network in 100+ countries worldwide

1990 Mediso founded	1994 Introduction of the first Mediso gamma camera	2000 Nucline™ X-ring/4R, 4-head dedicated brain SPECT	2006 Launching the first Mediso preclinical system the NanoSPECT/CT	2010 Launch of nanoScan® PET/CT, world's first ever sub-mm resolution preclinical PET/CT	2013 Mediso USA founded	2014 MultiScan™ LFER 150, world's first sub-mm resolution mobile PET/CT	2015 AnyScan™ TRIO SPECT, introduction of triple SPECT detector family	2016 Introducing the nanoScan™ PET/MRI 3T world's first superconducting preclinical PET/MRI	2018 Installation of the 100th nanoScan™ PET system	2022 Installation of the 300th preclinical imaging system	2023 Launch of the nanoScan™ MRI 7T and the PET Insert
------------------------	---	--	--	---	----------------------------	--	---	--	--	--	---



P 11

Exploiting the Vulnerabilities of Drug-resistant Lung Cancer with Antibody-drug Conjugates

AR Barber*, HE Greenwood, RS Edwards, WE Tyrrell, A Falzone, G DeNicola, TH Witney

School of Biomedical Engineering and Imaging Sciences, King's College London, St. Thomas' Hospital, London, UK; Department of Cancer Physiology, Moffitt Cancer Center, Tampa, FL 33612, USA.

* abigail.r.barber@kcl.ac.uk

Drug resistance continues to be a leading cause of therapeutic failure in lung cancer, highlighting an urgent need to develop new therapies with durable responses. Increasing evidence indicates transcriptional regulator NRF2 and downstream proteins, such as amino acid transporter xCT (Figure 1A), as key players in tumour drug resistance [1–4]. Here, we demonstrate the ability of [¹⁸F]FSPG to identify non-small cell lung cancer (NSCLC) tumours with high xCT expression *in vivo*. Subsequently, we validated an xCT-targeting monoclonal antibody (mAb) as a novel therapeutic agent to selectively target these drug-resistant NSCLC tumours.

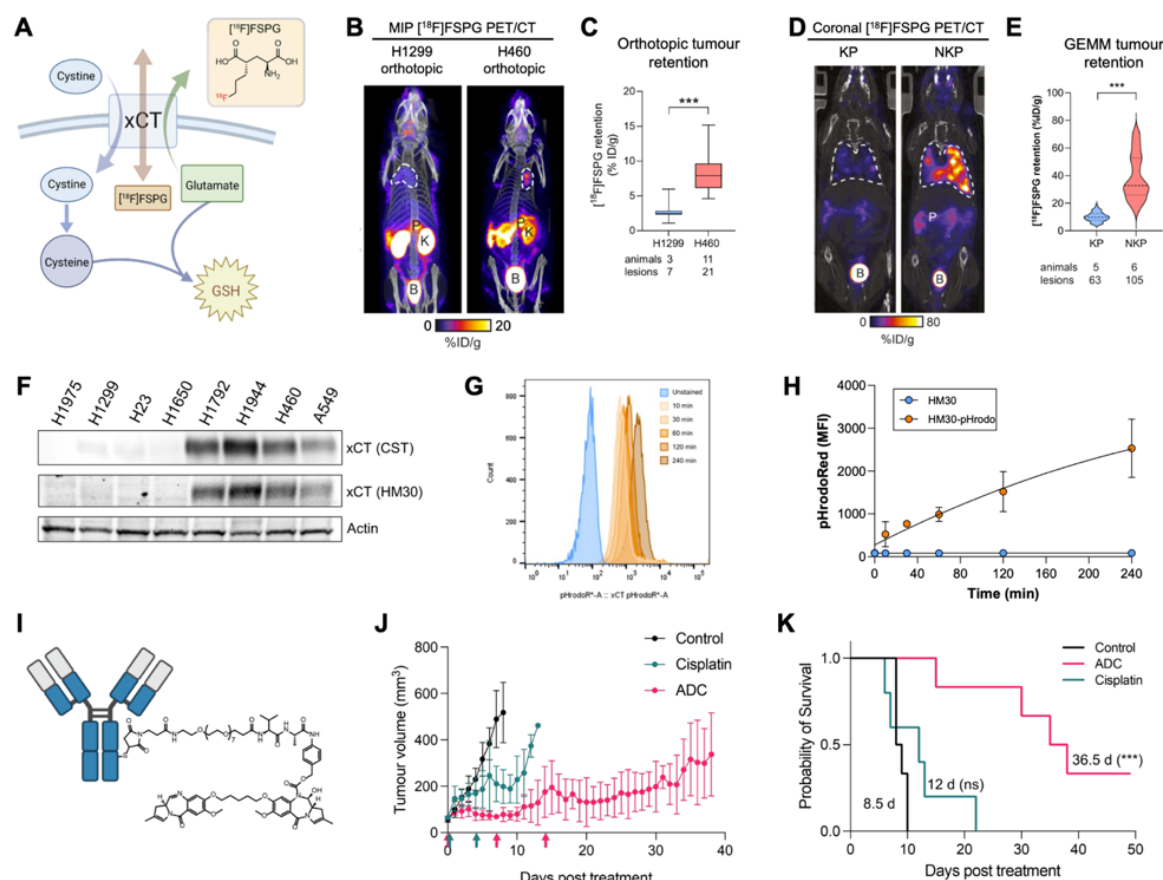


Figure 1. Elevated expression of xCT in drug-resistant lung cancer can be imaged by [¹⁸F]FSPG and therapeutically targeted using antibody-based strategies. **A.** A schematic of [¹⁸F]FSPG tumour retention through xCT. **B.** Representative sagittal PET/CT images in mice bearing orthotopic NSCLC tumours. Dotted white lines denote tumour borders; K, kidney; B, bladder; P, pancreas. **C.** Quantification of [¹⁸F]FSPG uptake in orthotopic NSCLC tumours. **D.** Representative coronal PET/CT images in genetically engineered mouse models (GEMM). **E.**

KP, Kras^{G12D}; p53^{flox/flox}; NKP, Nrf^{2D29H}. **E.** Quantification of [¹⁸F]FSPG uptake within lung lesions of KP and NKP mice. **F.** Western blot analysis of xCT expression in NSCLC cells using commercial (CST) and novel (HM30) antibodies. Actin was used as a loading control. **G.** Representative histogram of H460 cells incubated with pHrodo-Red-tagged HM30 over 4 hours. **H.** Quantification of pHrodo-Red fluorescence (n=3). **I.** Schematic representation of antibody-drug conjugate (ADC). **J.** Average tumour growth in mice bearing subcutaneous H460 tumours. Arrows indicate treatment administration (n=5/group). **K.** Kaplan-Meier plot demonstrating the probability of survival for each treatment group. ***, p<0.001.

PET imaging utilising [¹⁸F]FSPG can distinguish orthotopically grown xCT-high H460 tumours from xCT-low H1299 tumours (8.3±2.4%ID/g vs 2.8±1.5%ID/g, respectively; **Figure 1B/C**). In addition, [¹⁸F]FSPG retention was 3.6-fold higher in tumours with mutated Nrf2 (NKP) compared to WT Nrf2 (KP) (36.8±14.3%ID/g vs 10.1±3.3%ID/g, respectively; **Figure 1D/E**). The specificity of our xCT-targeting mAb was validated via western blot using a panel of NSCLC cell lines (Fig.1F). Internalisation studies were conducted by flow cytometry with mAb conjugated to a pH-sensitive fluorescent label. Antibody internalisation was confirmed, with an increase in fluorescence intensity facilitated by the low pH of lysosomes over a 4 h time course (**Figure 1G/H**). Subsequently, BALB/c nu/nu mice bearing ~70 mm³ subcutaneous H460 NSCLC tumours were treated with a novel antibody-drug conjugate (ADC) (**Figure 1I**), cisplatin or saline (n=5/group). The average tumour volume at seven days was lower in both cisplatin- and ADC-treated groups than in the control group (199mm³ and 78mm³ vs 518mm³, respectively; **Figure 1J**). ADC treatment significantly improved median survival compared to control and cisplatin groups (36.5 days vs 8.5 and 12 days, respectively, P<0.01; **Figure 1K**).

Here, we reveal that xCT and its upregulation by cancer cells can be noninvasively imaged by [¹⁸F]FSPG. This metabolic vulnerability can then be therapeutically targeted for sustained tumour growth suppression in NSCLC.

- [1] Tian Y, Liu Q, He X, Yuan X, Chen Y, Chu Q, et al. Emerging roles of Nrf2 signal in non-small cell lung cancer. *J Hematol Oncol.* 2016;9:14.
- [2] Briggs KJ, Koivunen P, Cao S, Backus KM, Olenchock BA, Patel H, et al. Paracrine Induction of HIF by Glutamate in Breast Cancer: EglN1 Senses Cysteine. *Cell.* 2016;166(1):126-39.
- [3] Ji X, Qian J, Rahman SMJ, Siska PJ, Zou Y, Harris BK, et al. xCT (SLC7A11)-mediated metabolic reprogramming promotes non-small cell lung cancer progression. *Oncogene.* 2018;37(36):5007-19.
- [4] Sugano K, Maeda K, Ohtani H, Nagahara H, Shibutani M, Hirakawa K. Expression of xCT as a predictor of disease recurrence in patients with colorectal cancer. *Anticancer Res.* 2015;35(2):677-82.

P 12

Multi-modal *In Vivo* Imaging for Lung Cancer Tracking

RCH Man*, SWS Leung, JKW Lam, GO Fruhwirth

¹King's College London

* chi.man@kcl.ac.uk

Lung cancer is the most common cancer worldwide and presents with high mortality [1]. For lung cancer therapeutics development, quantitative and non-invasive preclinical evaluation in traceable cancer models would be highly useful [2–4].

We lentivirally engineered *in vivo* traceable human non-small cell lung cancer NCI-H1975 cells with various reporter genes, either enhanced firefly luciferase (eFFly), human sodium iodide symporter (NIS) fused to a fluorescent protein, or equimolar levels of eFFly and NIS-GFP (exploiting 2A technology; **Figure 1A**). eFFly and/or NIS serves as whole-body imaging reporters while fluorescent proteins aided cell line generation and supported *ex vivo* validation. New traceable cell lines were characterized by flow cytometry, microscopy, and radiotracer uptake assays. Orthotopic lung tumour models in young-adult male immunodeficient NSG mice were established and tumour-bearing animals *in vivo* imaged (BLI, SPECT/CT) prior to *ex vivo* validation by histology.

Various NCI-H1975 reporter cell lines were successfully generated and purified through FACS (**Figure 1B**) and characterised *in vitro* for reporter expression, whereby we found reporters to separate as desired upon equimolar expression (**Figure 1A/C**) and to intracellularly localise as desired (**Figure 1D**). Whole-body imaging reporters were functional, i.e. generated bioluminescence from luciferin (**Figure 1E**) and took up [^{99m}Tc]TcO₄⁻ (**Figure 1F**). Serial BLI demonstrated tumour growth tracking in the lungs of tumour-bearing NSG mice (**Figure 2A**) while SPECT/CT revealed lung nodules (**Figure 2B**). Histology of harvested tumours confirmed sustained reporter expression and correlation with human CK-18 identifying tumour cells (**Figure 2C/D**).

In conclusion, we demonstrated successful engineering and validation of *in vivo* traceable human NCI-H1975 cell lines for use in future lung cancer therapeutics development. Equimolar expression of eFFly and NIS-GFP revealed eFFly-BLI to be more sensitive than NIS-SPECT/CT. While BLI will serve as a highly sensitive and cost-effective screening tool, the deep-lying nature of orthotopic lung cancer requires SPECT/CT that offers non-invasive and true 3D quantitation of treatment efficacy.

- [1] Wild, C., Weiderpass, E., & Stewart, B. W. (Eds.). (2020). World cancer report: cancer research for cancer prevention. International Agency for Research on Cancer.
- [2] Fruhwirth, G. O., Diocou, S., Blower, P. J., Ng, T., & Mullen, G. E. (2014). A whole-body dual-modality radionuclide optical strategy for preclinical imaging of metastasis and heterogeneous treatment response in different microenvironments. *Journal of Nuclear Medicine*, 55(4), 686-694.
- [3] Sanon S, Bos P D: *In Vivo* Imaging to Measure Spontaneous Lung Metastasis of Orthotopically-injected Breast Tumor Cells, *J Vis Exp* 2022; (184).

- [4] Volpe, A., Man, F., Lim, L., Khoshnevisan, A., Blower, J., Blower, P. J., & Fruhwirth, G. O. (2018). Radionuclide-fluorescence reporter gene imaging to track tumor progression in rodent tumor models. *JoVE* (Journal of Visualized Experiments), (133), e57088.

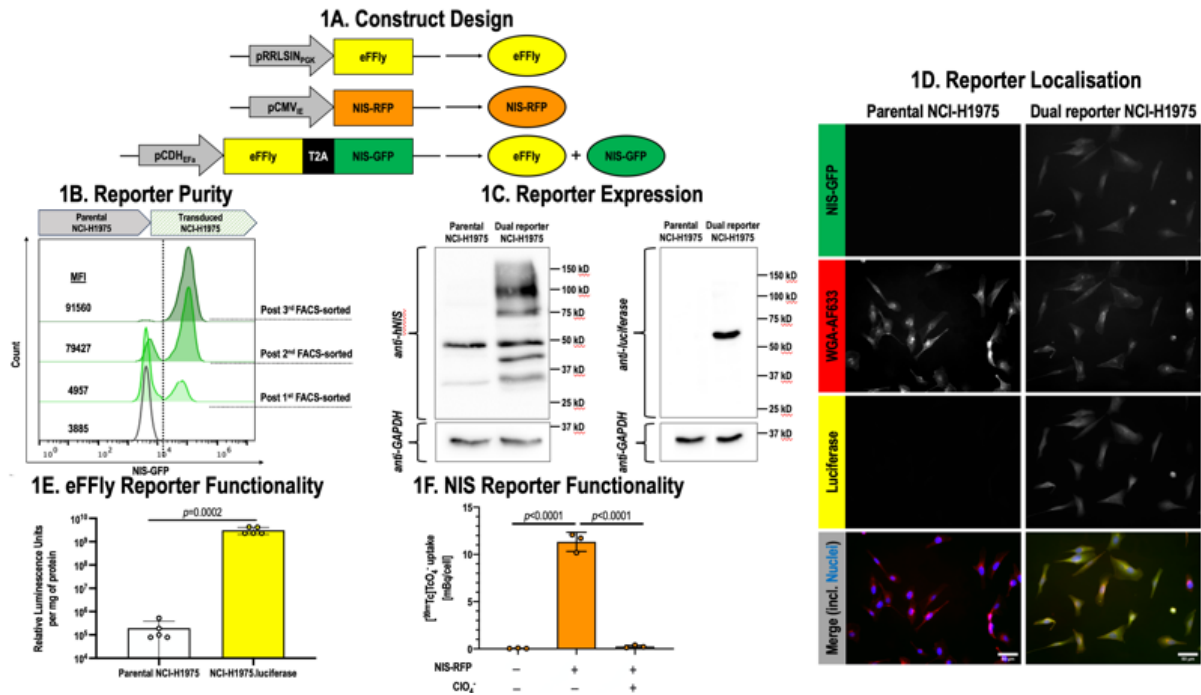


Figure 1. Engineering of a dual reporter NCI-H1975 cell line

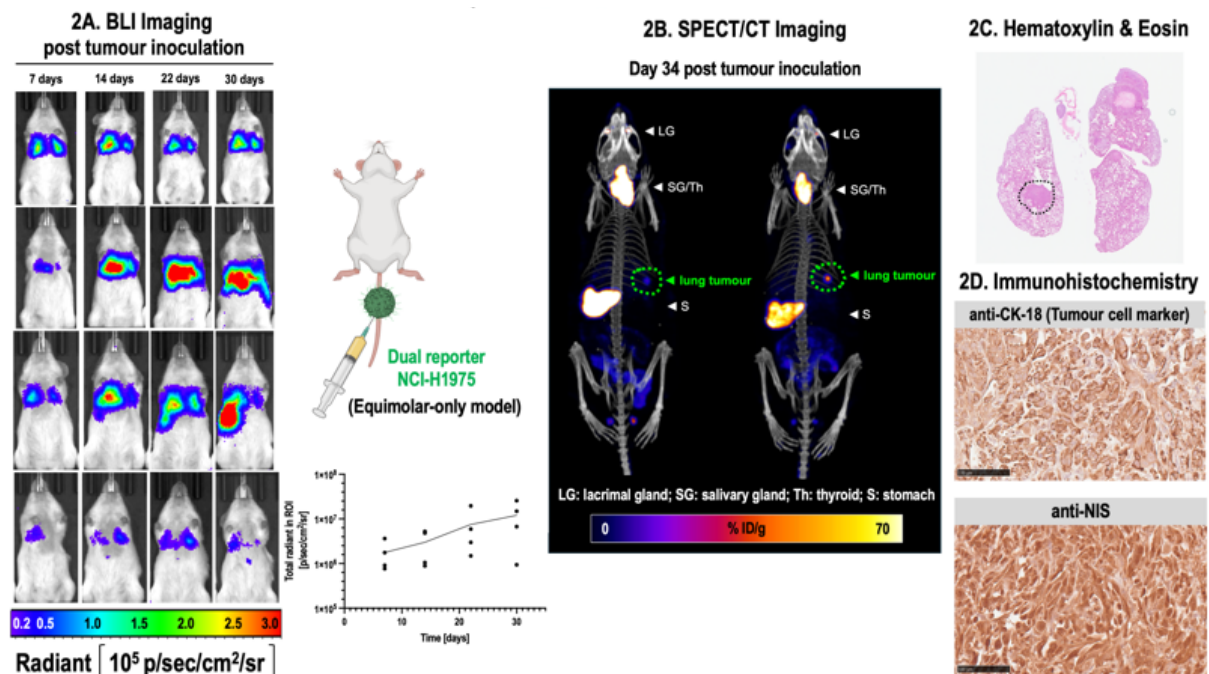


Figure 2. *In vivo* imaging in tumour-bearing NSG mice

P 13

Exploring the Role of LDH Isoforms in Prostate Cancer's Metabolism via [¹⁸F]FDG-PET/CT Imaging

M Farhangi*, J Goncalves Duarte, N Kuzhuppilly Ramakrishnan, J Kaggie, K Chary, L Aloj, F Gallagher

University of Cambridge

* mf805@cam.ac.uk

Normal prostate metabolism is unique, relying primarily on glycolysis to produce citrate for the seminal fluid fuelling spermatozoa. In contrast, early prostate cancer (PCa) favours oxidative metabolism, while advanced PCa reverts to glycolytic metabolism [1].

Lactate dehydrogenase (LDH), a key glycolytic enzyme, catalyses the conversion of pyruvate and lactate. LDH consists of four subunits, primarily encoded by *LDHA* and *LDHB* genes. These tetramers, labelled from LDH1 to LDH5, have differing amounts of A and B subunits, with all subunits of LDH1 being *LDHB* and all LDH5 being *LDHA*. Due to differences in substrate affinity (K_m), *LDHA*-derived isoforms preferentially catalyse the forward reaction from pyruvate to lactate, whilst *LDHB* favours the opposite [2]. PCa's LDH isoform expression could provide insights into shifts between anaerobic and aerobic metabolism. The concentration of LDH in prostate tissue plays a major role in determining the signal measured using hyperpolarised carbon-13 MRI following injection of hyperpolarised ¹³C-pyruvate [3,4]. It is less clear how changes in LDH may indirectly influence upstream glucose metabolism. We explored whether differences in LDH subunit expression can be detected through [¹⁸F]FDG-PET/CT.

CRISPR-Cas9 *LDHA* and *LDHB* gene knockouts (KO) were used to produce *in vivo* xenograft-tumour models, exploring the impact on glucose metabolism of PCa. In our pilot study, 18 tumour-bearing mice (control n=7, *LDHA* KO n=5, *LDHB* KO n=6) were imaged with [¹⁸F]FDG-PET/CT. Standard uptake value parameters (SUV_{max}, SUV_{mean}, SUV_{50%}, SUV_{75%}) were used to represent glucose uptake. We found a trend of higher [¹⁸F]FDG uptake and retention in *LDHA* KO tumours across all parameters (Figure 1). This could suggest that the absence of *LDHA* causes increased glucose uptake. Further studies increasing the sample size will assess whether this trend reaches statistical significance. Therefore,

[¹⁸F]FDG-PET may be able to indirectly probe changes in LDH expression in PCa.

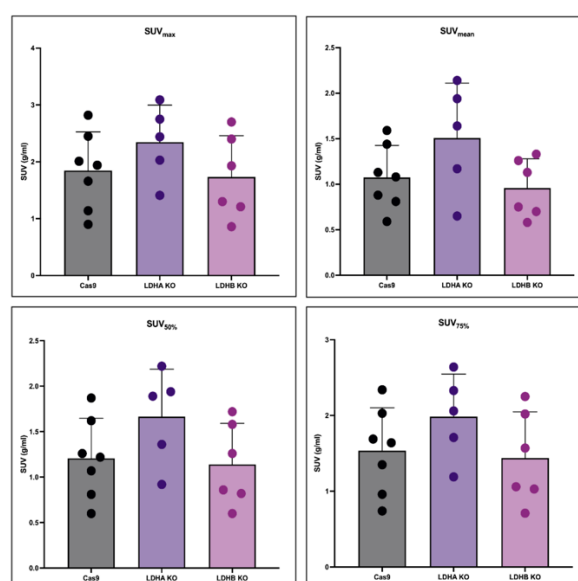


Figure 1. [¹⁸F]FDG standard uptake value parameters in control and *LDHA/B* KO mice

-
- [1] Wanjari, U. R. et al. Role of Metabolism and Metabolic Pathways in Prostate Cancer. *Metabolites* 13, 183 (2023).
 - [2] Farhana, A. & Lappin, S. L. Biochemistry, Lactate Dehydrogenase. in *StatPearls* (StatPearls Publishing, Treasure Island (FL), 2024).
 - [3] Sushentsev, N. et al. Hyperpolarised ¹³C-MRI identifies the emergence of a glycolytic cell population within intermediate-risk human prostate cancer. *Nat Commun* 13, 466 (2022).
 - [4] Sushentsev, N. et al. Metabolic imaging across scales reveals distinct prostate cancer phenotypes. *Nat Commun* 15, 5980 (2024).

P 14**Design and Synthesis of Fluorinated Carnitine Derivatives as Tools to Visualise Carnitine Utilisation and Metabolism**

RS Edwards*, E-M Hards, HE Greenwood, SN Dos Santos, M Tanc, TH Witney

Department of Imaging Chemistry and Biology, School of Biomedical Engineering and Imaging Sciences, King's College London, London, United Kingdom

* richard.edwards@kcl.ac.uk

Carnitine is essential for the transport of fatty acids from the cytosol into the mitochondrial matrix for β -oxidation and ATP synthesis [1]. Altered carnitine transport and metabolism are associated with multiple pathophysiological processes, including heart disease, cancer, and insulin resistance [2]. Imaging carnitine utilisation may reveal new insights into dysregulated fatty acid metabolism associated with these disease states. Here, we describe the design and synthesis of ^{19}F - and ^{18}F -labelled carnitine derivatives to measure carnitine transport and metabolism by NMR and PET.

$^{19/18}\text{F}$ Fluorinated carnitine derivatives were synthesised by fluoromethylation of their benzylester protected dimethyl amino precursors with fluoromethyltosylate ($^{19/18}\text{F}$ FMT), followed by deprotection of the benzyl group by either hydrogenation or hydrolysis. Purification was achieved using a weak cation exchange resin. Analysis of the radiofluorination reactions and products was conducted using radio-HPLC.

Dynamic PET/CT imaging (Mediso) was performed following i.v. injection of ~ 1.5 MBq ^{18}F fluoromethyl-carnitine (^{18}F FMC) or ^{18}F fluoromethyl- γ -butyrobetaine (^{18}F FMGBB) in healthy mice ($n=4/\text{group}$). Lastly, PET/CT imaging was performed following a simultaneous injection of ^{18}F FMC and $0.56 \mu\text{mol}$ of carnitine ($50 \mu\text{L}$, Sigma) to generate a blood concentration of $\sim 400 \mu\text{M}$.

Fluorinated carnitine derivatives were designed to exhibit both the transport (via OCTN2) and metabolic activity of their natural equivalents. These fluorinated carnitine derivatives were synthesised in 3 steps from their dimethyl amino derivatives. The final products were isolated using a weak cation exchange resin with $>95\%$ purity, providing simple and rapid access to the different analogues. This method was adapted for a 3 step radiosynthesis: ^{18}F FMT production, fluoromethylation, and deprotection. Radiochemical yields were $>10\%$. ^{18}F FMC was stable over 3h. The radiofluorinated carnitine derivatives ^{18}F FMC and ^{18}F FMGBB were used to visualise carnitine and γ -butyrobetaine utilisation in healthy mice. Both radiotracers showed high kidney and liver retention with urinary excretion only observed for ^{18}F FMGBB (**Figure 1A–D**). Importantly, heart uptake of ^{18}F FMC was blocked by $\sim 50\%$ following co-administration of carnitine (**Figure 1E/F**).

A simple 3 step method has been developed to allow rapid access to both ^{19}F - and ^{18}F -labelled carnitine derivatives, which retain both transport and metabolic activity. PET imaging of ^{18}F FMC and ^{18}F FMGBB enabled visualisation of differences in the distribution of carnitine and its biosynthetic precursor, γ -butyrobetaine. Furthermore, ^{18}F FMC distribution and uptake was altered by perturbing the concentration of endogenous carnitine.

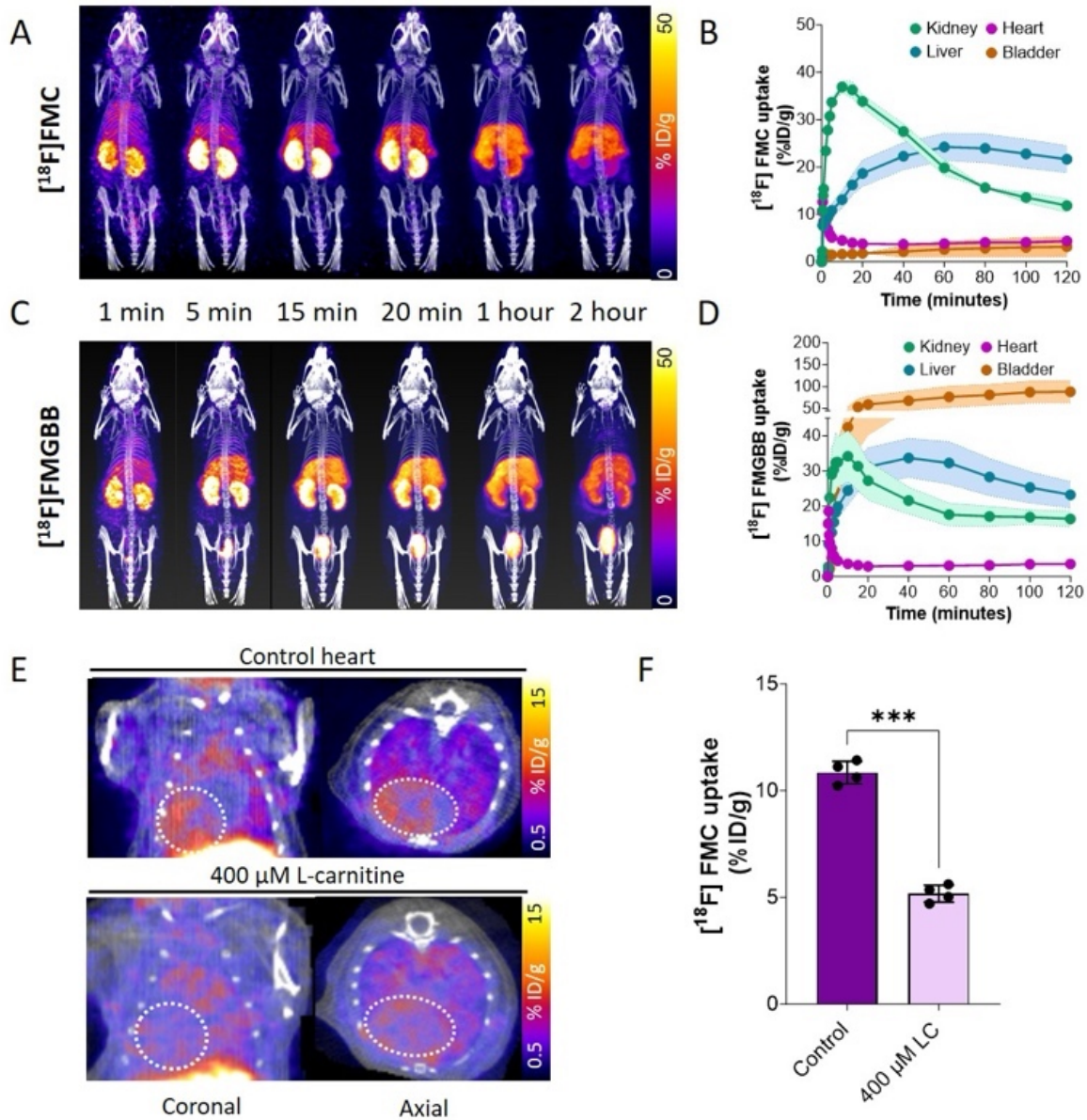


Figure 1. Visualisation of carnitine and γ -butyrobetaine utilisation in healthy mice using the radiofluorinated carnitine derivatives $[^{18}\text{F}]\text{FMC}$ and $[^{18}\text{F}]\text{FMGBB}$

- [1] Longo N, Amat di San Filippo C, Pasquali M. Disorders of carnitine transport and the carnitine cycle. *Am J Med Genet C Semin Med Genet.* 2006, 142C(2), 77-85
- [2] Dambrova M, Makrecka-Kuka M, Kuka J, et. al. Acylcarnitines: Nomenclature, Biomarkers, Therapeutic Potential, Drug Targets, and Clinical Trials. *Pharmacol Rev* 2022, 74, 506–551

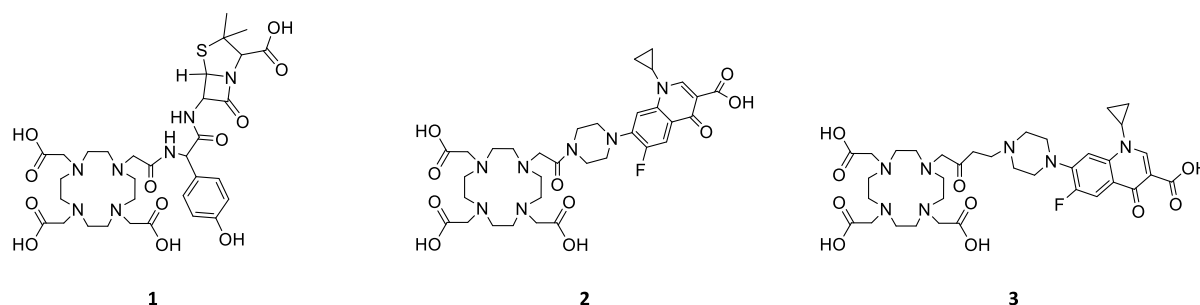
P 15

Assessing the Biodistribution and Localisation of Antibiotics Using Molecular Imaging

R Al-Zuhairi^{1,2,*}, J Domarkas^{1,2}, J Wright^{1,2,3}, I Renard^{1,2,3}, G Efthimiou², B Abdulwahaab^{1,2}, SJ Archibald^{1,2,3}¹PET Research Centre, University of Hull; ²Centre for Biomedicine, Hull York Medical School; ³School of Biomedical Engineering and Imaging Sciences, King's College London

* R.M.AL-ZUHAIRI-2020@hull.ac.uk

Identification of the anatomical location of infections using imaging is important to allow effective treatment and, equally important, is the accumulation of antibiotic therapies at the site of infection. Conjugation of antibiotics to increase uptake at target sites or organs could offer significantly improved therapeutic response. As a proof of concept, two widely used antibiotics, ciprofloxacin and amoxicillin, were derivatised to conjugate a DO3A chelator¹ and allow subsequent radiolabelling with ⁶⁸Ga for PET imaging. The properties of the antibiotic conjugates **1**, **2** and **3** (**Figure 1**). Cytotoxicity investigation of **1** and **3** in *Staphylococcus aureus* and *Acinetobacter baumannii* cultures showed Minimum Inhibitory Concentrations (MICs) from 50 µg/mL of **1** and 25 µg/mL of **3** in *S. aureus* and 25 µg/mL of **1** and 50 µg/mL of **3** in *A. baumannii* and a Minimum Bactericidal Concentration (MBC) of 200 µg/mL and 100 µg/mL for **1** and **3**, respectively, in both species. ⁶⁸Ga-radiolabelling of the three antibiotic derivatives was achieved with radiochemical yields of 55%, 98% and 95% for [⁶⁸Ga]Ga**1**, [⁶⁸Ga]Ga**2** and [⁶⁸Ga]Ga**3**, respectively. *In vitro* bacteria uptake of [⁶⁸Ga]Ga**2** and [⁶⁸Ga]Ga**3** in *S. aureus* showed radiotracer uptake up to 17% for [⁶⁸Ga]Ga**2** and 21% for [⁶⁸Ga]Ga**3**. A noticeable reduction of tracer uptake was observed following pre-incubation with a blocking dose of Ga(NO₃)₃ (8 mM). PET/CT imaging of [⁶⁸Ga]Ga**2** and [⁶⁸Ga]Ga**3** in naïve animals showed rapid renal excretion with no tissue retention, warranting further development of targeted conjugates and evaluation in preclinical models of infection.

**Figure 1.** Structures of antibiotic conjugates **1–3** for radiolabelling with ⁶⁸Ga

- [1] Stvolinsky, S.; Antonova, N.; Kulikova, O.; *et al.*: Synthesis, Study of Physico-Chemical and Antioxidant Properties, Biological Activity. *Biochemistry (Moscow), Supplement Series B: Biomedical Chemistry* 2018, 12, 308-315.
- [2] Koźmiński, P.; Gawęda, W.; Rzewuska, M.; *et al.* Physicochemical and biological study of ^{99m}Tc and ⁶⁸Ga radiolabelled ciprofloxacin and evaluation of [^{99m}Tc]Tc-CIP as potential diagnostic radiopharmaceutical for diabetic foot syndrome imaging. *Tomography* 2021, 7 (4), 829-842.

P 16

Evaluation of Blood Pool Albumin-binding PET Radiopharmaceuticals for Cardiac Functional Imaging

J Koch-Paszkowski^{1,*}, J Domarkas¹, E Ramou¹, N Lawrence¹, JD Wright^{1,2}, L Allott¹, T Palmer¹, R Southworth², SJ Archibald^{1,2}

¹Centre for Biomedicine and Positron Emission Tomography Research Centre, Hull York Medical School and University of Hull, Cottingham Road, Hull, UK; ²School of Biomedical Engineering and Imaging Sciences, King's College London, 4th Floor Lambeth Wing, St Thomas' Hospital, London SE1 7EH, UK

* j.koch-paszkowski@hull.ac.uk

Cardiac functional imaging is used to diagnose and monitor cardiovascular injury. One of the functional imaging methods is a multi-gated acquisition scan (MUGA). In MUGA blood pool agent, (^{99m}Tc)-pertechnetate-labelled-red blood cells (RBC)), is used to acquire gated images and establish cardiac output. Positron emission tomography (PET) blood pool agents [1,2] could be used as an alternative, allowing higher sensitivity. Using albumin-binding blood pool radiopharmaceuticals eliminates the step of RBC labelling and enables prolonged circulation in vasculature. This study aims to develop and evaluate several PET albumin-binding radiopharmaceuticals for MUGA imaging in preclinical settings.

Three compounds α - ^{18}F F- ω -phenylBu-PEG6, non-albumin binding analogue α - ^{18}F F- ω -N3-PEG6 and α - ^{68}Ga Ga-DO3A- ω -4-tolylBu-PEG6 were prepared from their tosylated or DO3A functionalised precursors. Their binding to bovine serum albumin (BSA) (Gibco, USA) was evaluated using a size exclusion differentiation on a PD-10 column (Minitrap G-25, Cytiva, USA). The washout patterns from the column were compared with ^{89}Zr Zr-DFO-BSA (pure albumin compound) and 3.25% BSA. Stability, up to 4 h at 37°C in PBS and rat serum (Invitrogen, USA) formulation of ^{18}F -fluorinated radiopharmaceuticals was confirmed. Gamma counting was used to measure LogD7.4 of α - ^{18}F F- ω -phenylBu-PEG6 and α - ^{68}Ga Ga-DO3A- ω -4-tolylBu-PEG6, which were found to be lipophilic and hydrophilic, respectively. The blood pool clearance of ^{89}Zr Zr-DFO-BSA was established during dynamic PET/CT imaging of naïve mice, followed by static imaging at 270 mins post-injection (**Figure 1**). Dynamic ^{68}Ga Ga-DOTA PET/CT imaging was performed to establish the biodistribution of the non- conjugated gallium-68 chelator complex as a control.

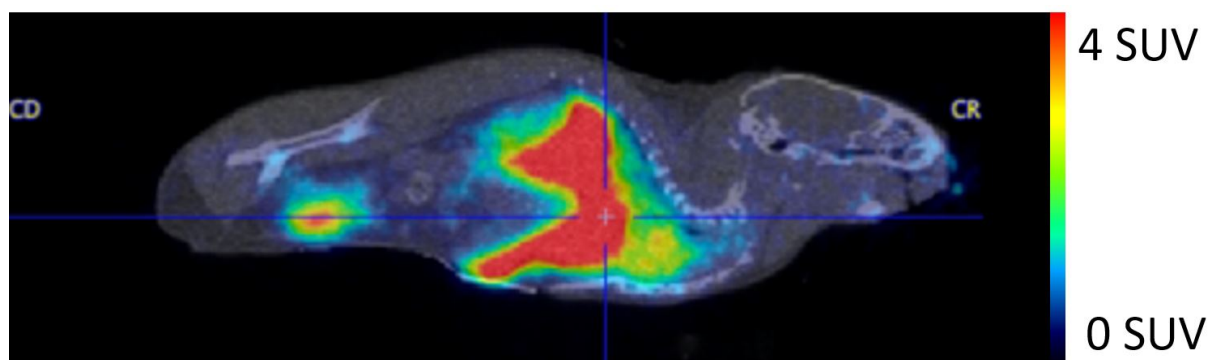


Figure 1. ^{89}Zr Zr-DFO-BSA scan of naïve mouse 1h p.i.

α -[^{18}F]F- ω -phenylBu-PEG6 and α -[^{68}Ga]Ga-DO3A- ω -4-tolylBu-PEG6 showed binding to isolated albumin *in vitro*. As expected, α -[^{18}F]F- ω -N3-PEG6 did not bind to albumin. [^{89}Zr]Zr-DFO-BSA remained in blood pool for up to 270 mins, whilst [^{68}Ga]Ga-DOTA was rapidly cleared. The next steps of the study will include further evaluation of the radiopharmaceutical–protein interaction *in vitro* and *in vivo*, followed by a biodistribution study of [^{18}F]-fluorine-labelled and [^{68}Ga]-gallium-labelled radiopharmaceuticals *in vivo*.

- [1] Matsusaka Y, Nakahara T, Takahashi K, Iwabuchi Y, Nishime C, Kajimura M, et al. F-18-FDG-labeled red blood cell PET for blood-pool imaging: preclinical evaluation in rats. EJNMI Research. 2017;7
- [2] Zhang JJ, Lang LX, Zhu ZH, Li F, Niu G, Chen XY. Clinical Translation of an Albumin-Binding PET Radiotracer ^{68}Ga -NEB. J Nucl Med. 2015;56(10):1609-14

P 17**Quantitative *In Vivo* Detection of Mitochondrial and Sarcolemmal Membrane Potential Derived from the Pharmacokinetics of Radiolabelled Lipophilic Cations**

E Waters*, R Southworth, T Eykyn

King's College London

* edward.waters@kcl.ac.uk

[^{99m}Tc]Sestamibi (MIBI) is lipophilic and cationic, therefore its cellular distribution and tissue retention is governed by the negative potential differences across the sarcolemmal ($\Delta\Psi_s$) and mitochondrial ($\Delta\Psi_m$) membranes. Here we present the first *in vivo*, quantitative, non-invasive measurement of $\Delta\Psi_s$ and $\Delta\Psi_m$ using a novel kinetic modelling approach (**Figure 1**). We developed and validated our model in isolated Langendorff-perfused hearts, then using MIBI planar scintigraphy we fitted our model to cardiac time-activity curves and measured $\Delta\Psi_s$ and $\Delta\Psi_m$ *in vivo* for the first time.

We pharmacologically depolarise both $\Delta\Psi_s$ and $\Delta\Psi_m$ to rigorously test the models ability to quantify these parameters (**Figure 2**). During normal perfusion we measured $\Delta\Psi_s = -69 \pm 1$ mV and $\Delta\Psi_m = -100 \pm 4$ mV. During hyperkalaemia, measured $\Delta\Psi_s$ fell sequentially with increasing K⁺ concentration to -46 ± 2 mV at [K⁺] = 25 mM, whilst $\Delta\Psi_m$ was unchanged at -104 ± 5 mV. In hearts treated with 300nM of the ionophore CCCP, $\Delta\Psi_s = -71 \pm 7$ mV was unchanged while $\Delta\Psi_m = -56 \pm 17$ mV was depolarised, while with 600nM CCCP $\Delta\Psi_s = -55 \pm 4$ mV was reduced and $\Delta\Psi_m = -6 \pm 2$ mV was completely dissipated. *In vivo*, we measured $\Delta\Psi_s = -67.4 \pm 6.8$ mV (n=4, \pm SD) and $\Delta\Psi_m = 154.3 \pm 6.1$ mV.

We quantified $\Delta\Psi_s$ and $\Delta\Psi_m$ from cardiac time activity curves of MIBI *in vivo* and in isolated rat hearts, and measured $\Delta\Psi_s$ and $\Delta\Psi_m$ when one or other of the membranes is depolarised. This shows the potential to detect mitochondrial membrane potentials *in vivo* clinically. This could have broad application in the pathophysiology of heart failure, monitoring the cardiotoxicity of chemo and radiotherapy and the diagnosis of age-related diseases.

- [1] Safee ZM, Baark F, Waters ECT, et al (2019) Detection of anthracycline-induced cardiotoxicity using perfusion-corrected ^{99m}Tc sestamibi SPECT. Sci Rep 9:216
- [2] Crane P, Laliberté R, Heminway S, et al (1993) Effect of mitochondrial viability and metabolism on technetium-99m-sestamibi myocardial retention. Eur J Nucl Med 20:20–25
- [3] Handley MG, Medina RA, Mariotti E, Kenny GD, Shaw KP, Yan R, et al. Cardiac Hypoxia Imaging: Second-Generation Analogues of ⁶⁴Cu-ATSM. Journal of Nuclear Medicine. 2014;55(3):488–95
- [4] Logan A, Pell VR, Shaffer KJ, Evans C, Stanley NJ, Robb EL, et al. Assessing the mitochondrial membrane potential in cells and *in vivo* using targeted click chemistry and mass spectrometry. Cell Metab. 2016;23(2):379–85

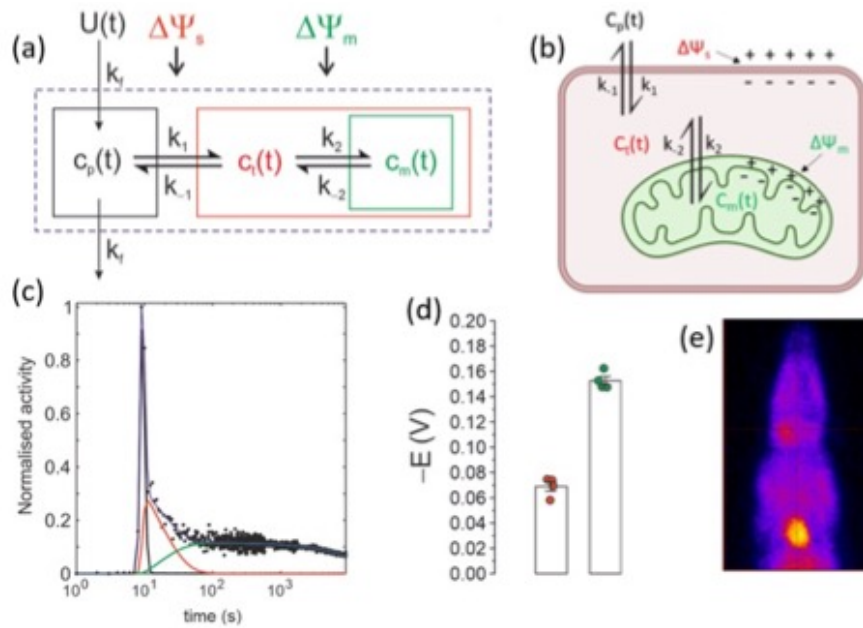


Figure 1. (a) Model used to fit MIBI time-activity curves; (b) diagram depicting how modelled parameters inform on sub-cellular radiotracer distribution; (c) example fit of time-activity curve acquired from planar scintigraphy imaging measured from ROI drawn around heart; (d) $\Delta\Psi_s$ and $\Delta\Psi_m$ measured from the modelling of time-activity curves; (e) example frame of a planar scintigraphy scan.

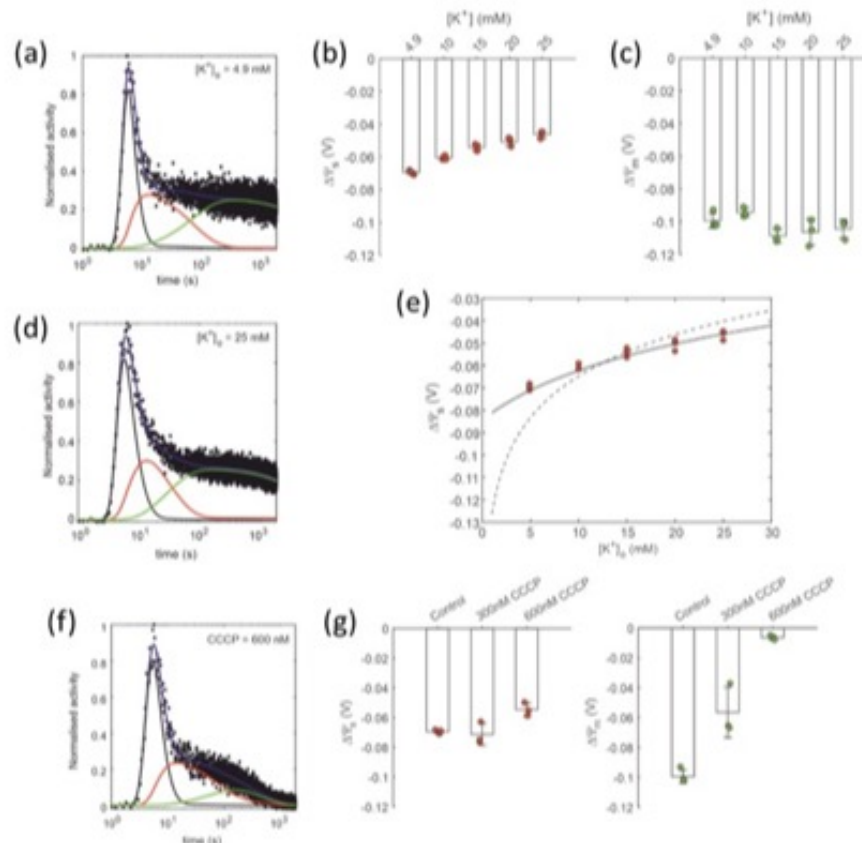


Figure 2. (a) Example of fit in normally perfused heart; (b) $\Delta\Psi_s$, measured from hearts perfused with different concentration of K^+ ; (c) $\Delta\Psi_m$ of hearts perfused with different concentration of K^+ ; (d) example of fit in heart perfused with high K^+ concentration (25 mM); (e) measured $\Delta\Psi_s$ overlaid on curves predicted by Goldman-Hodgkin-Katz equation (solid line) and Boltzman equation (dotted line); (f) example of fit in heart perfused with CCCP (600 nM); (g) $\Delta\Psi_s$ and $\Delta\Psi_m$ of hearts perfused with different CCCP concentrations.

P 18

Imaging-guided Development of Polysarcosine-based Star Dendrimers for Drug Delivery

T Gibson, A Mishra, A Carrascal Minino, T Floyd, J Pellico, M Mazza, TH Witney, R TM de Rosales*

School of Biomedical Engineering and Imaging Sciences, King's College London, London, United Kingdom

* rafael.torres@kcl.ac.uk

Polysarcosine (pSar)-based star dendrimers (SDends) are under investigation for drug delivery applications. Comprising of pSar functionalised G5-PLL dendrimers, precise, high-capacity drug loading is possible, achieving prolonged circulation times *in vivo*, owing to the stealth properties of the PEG alternative, pSar. To inform their development and better understand the role of pSar on biodistribution and pharmacokinetics, we investigate the *in vivo* behaviour of three pSar SDends by PET/CT.

Three SDends with different pSar chain lengths (SD28, SD56 and SD100) were synthesised [1], minimally functionalised at the core with deferoxamine and Alexafluor647 and radiolabelled with zirconium-89 (^{89}Zr) (Figure 1). SDends were administered to healthy female BALB/c mice and PET/CT images obtained over 96h.

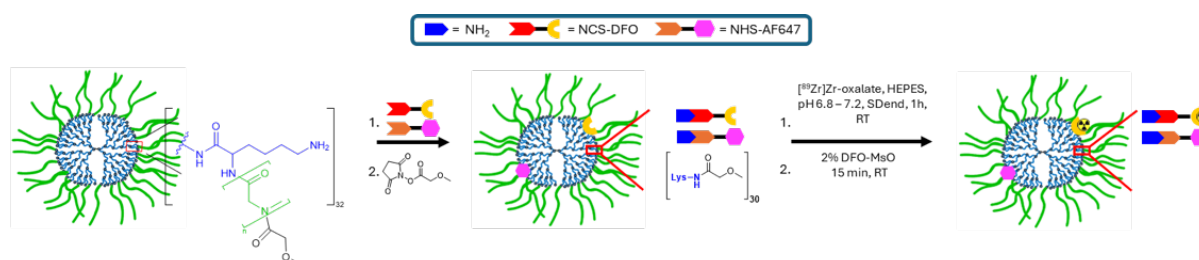


Figure 1. Schematic representation of the functionalisation and radiolabelling protocol for pSar SDends. SDends were modified with one molecule of DFO and AF647 per particle via the ϵ -amine of the PLL core and residual ϵ -amines capped to yield charge neutral methoxy groups. Radiolabelling with ^{89}Zr is achieved under ambient conditions to yield particles for *in vivo* imaging

SDends were synthesised with molecular weights of 73.4, 131.3 and 286.4 kDa and hydrodynamic diameters of 10.2, 14.1 and 21.9 nm as determined by MALDI-TOF/GPC and DLS respectively (Figure 2a–b). Radiolabelling with ^{89}Zr is achieved with high radiochemical yields (>73%), high radiochemical purities (>95%) and >50% radiochemical stability in PBS and serum after 72h (Figure 2c–f). PET/CT images show high blood circulation at early time points followed by progressive uptake by the reticuloendothelial system (Figure 3a). Importantly, particles are still in blood circulation after 96h, achieving prolonged blood circulation with increasing pSar chain length (10.9, 16.6 and 18.2 %IA/g in blood after 96 h for SD28, SD56 and SD100, respectively; Figure 3b), highlighting the stealth ability of pSar. The long circulation time of these DDSs suggest they will accumulate readily in tumours.

We present a facile method to radiolabel novel SDends with ^{89}Zr with high radiochemical yield, purity and stability. *In vivo* PET imaging highlights the ability of pSar SDends to sufficiently

evade the immune system with significant retention in blood circulation after 96h. Future studies will evaluate the tumour uptake and biodistribution upon repeat administration.

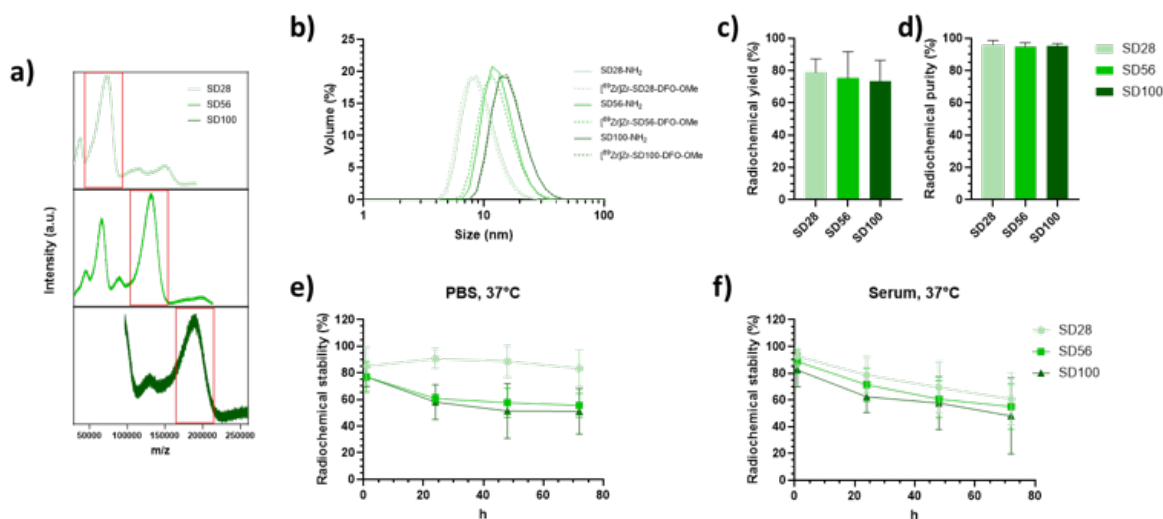


Figure 2. (a) MALDI-TOF-MS spectra, highlighted are the peak maximum molar mass (Mp) regions for each SDend; (b) Hydrodynamic diameters of pSar SDends pre- and post- radiolabelling, as determined by DLS, data represent the mean (n= 3); (c) Radiochemical yields, data represent the mean \pm SD (n= 3); (d) radiochemical purity, data represent the mean \pm SD (n= 3); (e) radiochemical stability in PBS over 72 h, data represent the mean \pm SD (n= 3); (f) radiochemical stability in serum over 72 h, data represent the mean \pm SD (n= 3).

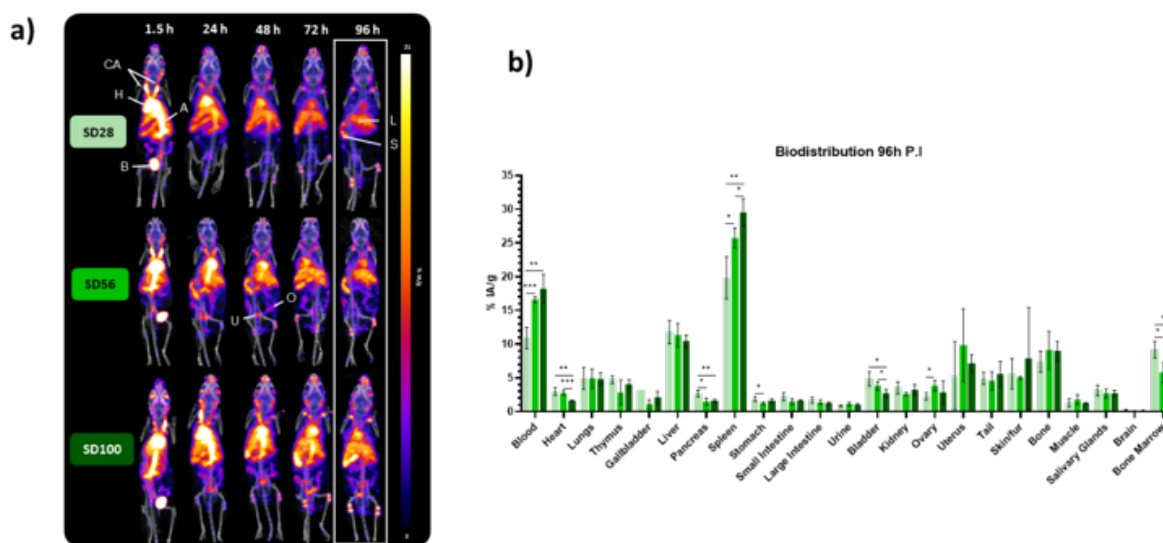


Figure 3. (a) Maximum intensity projection PET/CT images after I.V injection of $^{89}\text{Zr}/\text{AF647}$ labelled SDends ($\sim 2\text{--}3$ MBq, ca. 2.5×10^{15} particles) in healthy female BALB/c mice, (12-13 weeks, n= 4 per group) at 1.5, 24, 48, 72 and 96 h P.I. CA= Carotid Artery, H= Heart, A= Aorta, B= Bladder, L= Liver, S= Spleen, U= Uterus, O= Ovary; (b) ex vivo biodistribution distribution data as determined by gamma counting. Organs harvested 96 h P.I following organ perfusion. Data expressed as percentage of injected activity (activity in organ/total injected activity) per gram of tissue. Data represent the mean \pm SD (n= 4). P values: * < 0.05, ** < 0.01, *** < 0.001

[1] England, R. M., Moss, J. I., Gunnarsson, A., Parker, J. S. & Ashford, M. B. Synthesis and Characterization of Dendrimer-Based Polysarcosine Star Polymers: Well-Defined, Versatile Platforms Designed for Drug-Delivery Applications. *Biomacromolecules* 21, 3332–3341 (2020).

P 19

Exploring Hyaluronan Nanocapsules as PARP Inhibitor Delivery Systems: *In Vitro* and *In Vivo* Studies (SPECT) in Healthy Mice

J Tang*, J Pellico Saez, A Minino, A Mishra, MJ Alonso, S Terry, R TM de Rosales

School of Biomedical Engineering and Imaging Sciences, King's College London, London, United Kingdom

* jie.2.tang@kcl.ac.uk

The goal of this research is to improve the biodistribution properties and tumour accumulation of poly ADP-ribose polymerase inhibitors (PARPis) via novel drug delivery systems for more efficient anti-cancer treatments. In this study we explored hyaluronan nanocapsules (NCs) [1], as potential PARPi drug delivery systems *in vitro* and *in vivo* [1] using [¹²⁵I]I-PARPi as a tracer for SPECT imaging.

I-PARPi was chosen after comparing the similar radiosensitising effects compared to Olaparib and F-PARPi, whilst allowing long-term tracking using ¹²⁵I SPECT imaging. [¹²⁵I]I-PARPi NCs were synthesised following previous methods [1,2] and using [¹²⁵I]I-PARPi/I-PARPi in the organic phase. Size-exclusion chromatography indicated high (>80 %) encapsulation efficiency (EE) that was not affected by the amount of drug (I-PARPi) loaded in the NCs. Negative control studies verified the EE results. [¹²⁵I]I-PARPi NCs were colloidal and radiochemically stable in human serum and showed slow drug release over 72h *in vitro*. We then evaluated the biodistribution of [¹²⁵I]I-PARPi and [¹²⁵I]I-PARPi NCs in healthy Balb/c mice via SPECT imaging (2, 6 and 24 h) and *ex vivo* biodistribution studies (24h only). At early (2h) timepoints, the biodistribution of [¹²⁵I]I-PARPi and [¹²⁵I]I-PARPi NCs showed no significant differences in blood circulation, but significant differences in liver uptake, consistent with the behaviour of nanoparticulates. At later timepoints (24h), however, the biodistribution differed to what could be expected for a particulate drug delivery system with [¹²⁵I]I-PARPi showing higher levels of retention in liver/spleen, and higher thyroid levels for [¹²⁵I]I-PARPi NCs, which is likely the result of increased release of free [¹²⁵I]I-iodide (**Figure 1**).

Hyaluronan NCs appear to be a good system to encapsulate and slowly release PARPi *in vitro*. However, the [¹²⁵I]I-PARPi NCs seem to release the drug at a much faster rate *in vivo* making Hyaluronan NCs suboptimal for future applications as a PARPi delivery system. Future work will be looking for alternative nanocarriers for PARPi.

- [1] Molina-Crespo, Ángela, et al. "Intracellular Delivery of an Antibody Targeting Gasdermin-B Reduces HER2 Breast Cancer Aggressiveness Targeted Anti-Gasdermin-B Nanotherapy in HER2 Breast Tumors." *Clinical Cancer Research* 25.15 (2019): 4846-4858
- [2] Reilly, Sean W., et al. "Rapid Cu-catalyzed [²¹¹At] astatination and [¹²⁵I] iodination of boronic esters at room temperature." *Organic letters* 20.7 (2018): 1752-1755
- [3] Pirovano, Giacomo, et al. "Targeted Brain Tumor Radiotherapy Using an Auger Emitter PARP1-targeted Auger Radiotheranostic in Glioblastoma." *Clinical Cancer Research* 26.12 (2020): 2871-2881

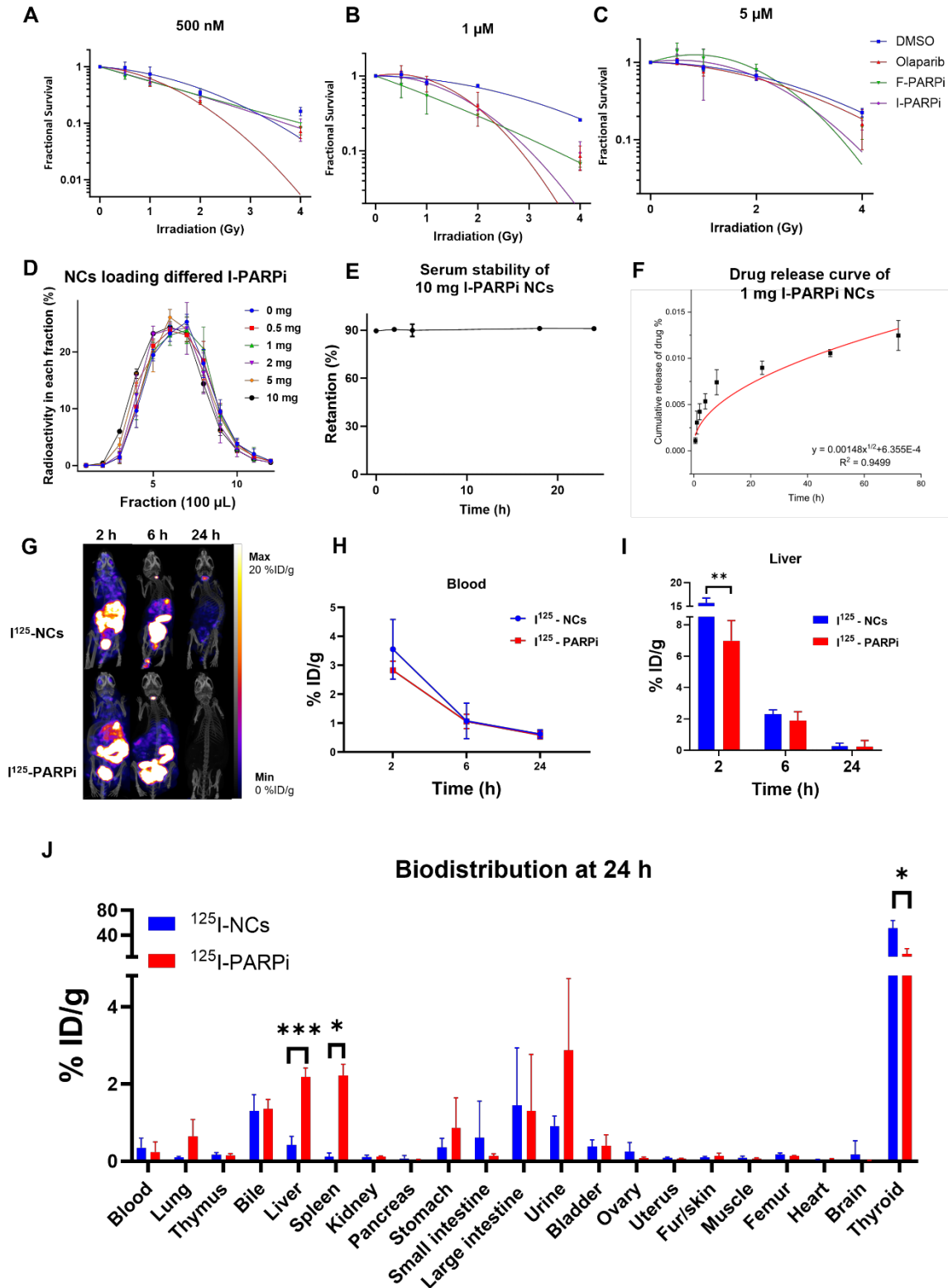


Figure 1. Characterisation of hyaluronan NCs as delivery system for $[^{125}\text{I}]\text{I-PARPi}$

P 20

Count Rate Performance of a PET Tracer on a Preclinical SPECT System with Multipinhole Collimators

AM Drews*, M Kovacs, TH Witney, P Marsden, L Livieratos

School of Biomedical Engineering and Imaging Sciences, King's College London; Mediso Medical Imaging Systems

* allen.drews@kcl.ac.uk

Recent advances in SPECT detector technology have led to systems being able to measure radionuclide gamma emissions of up to 600 keV, allowing capture of the 511 keV annihilation gamma rays of tracers previously only used in PET. It is of interest to study how SPECT systems respond to these high energy photons compared to traditional low-energy tracers like ^{99m}Tc . A particular aspect of interest is whether at high-input count rates a linear detector response is maintained. Linearity is essential for quantitative image analysis and may be exceeded in applications with a wide range of count rates, such as, high-throughput multi-animal imaging or longitudinal dynamic imaging.

We report phantom-based system count rate linearity measurements for a preclinical SPECT/CT system equipped with novel low- and high-energy multipinhole collimators. Measurements were performed with point- and cylinder sources across an activity range from ~ 200 MBq to <0.1 MBq for ^{99m}Tc and ^{18}F . For ^{99m}Tc , standard-energy MPH collimators (up to 300 keV) were used, while for ^{18}F , next generation high-energy MPH collimators (300 – 600 keV) were used. The detected count rate and reconstructed image uniformity were analysed.

For both radionuclides and collimator sets, the measured count rate was linear over the range tested. For ^{18}F , count rate showed zero loss for the entire range of input activities. For ^{99m}Tc , count rate losses of 10% only occurred at 127 MBq. Reconstructed images showed accurate quantification across the range of input activities, with $<5\%$ quantification errors below 100 MBq for ^{99m}Tc . Reconstructed image uniformity only degraded at low input activities of <1 MBq (**Figure 1**).

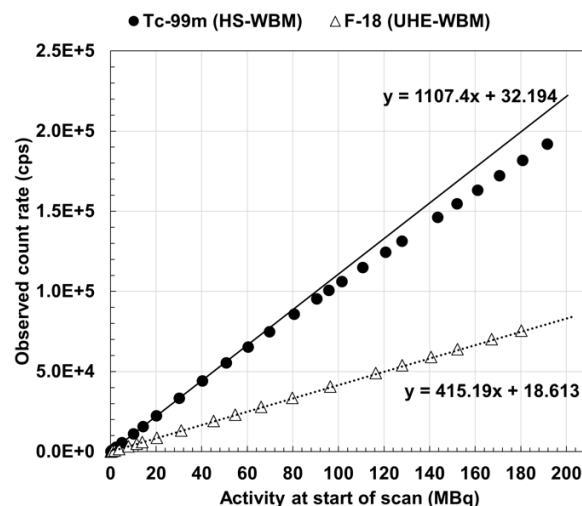


Figure 1. Correlation of measured radioactivity and detected count rate

We conclude that the chosen SPECT system provides excellent count rate linearity for the test conditions (point sources in air, distributed source) for both ^{99m}Tc and ^{18}F over a larger range of input activities.

P 21

Establishment of Diagnostic Reference Levels for Computed Tomography Examination at the University of Ghana Medical Centre

S Issahaku, I Kwesi Acquah*, S Mensah Amoh, G Nunoo

University of Education, Winneba, University of Ghana

* acquah919@gmail.com

Diagnostic Reference Levels are important indicators for monitoring and optimizing protocol and procedure in medical imaging between facilities and equipment. This helps to evaluate whether, in routine clinical conditions, the median value obtained for a representative group of patients are within an agreed range from a specified procedure is unusually high or low for that procedure. This study aimed to propose Diagnostic Reference Levels for Computed Tomography examination of the most common routine examination of the head, chest and abdominal pelvis regions at the University of Ghana Medical Centre.

The Diagnostic Reference Levels were determined based on the investigation of the most common routine examinations including head Computed Tomography examination with and without contrast, abdominopelvic Computed Tomography examination with and without contrast, and chest Computed Tomography examination without contrast. The study was based on two dose indicators; the volumetric Computed Tomography Dose Index and Dose-Length Product.

The estimated median distribution for head Computed Tomography with contrast for volumetric-Computed Tomography dose index and Dose-Length Product were 38.33 mGy and 829.35 mGy.cm, while without contrast, were 38.90 mGy and 860.90 mGy.cm respectively. For an abdominopelvic Computed Tomography examination with contrast, the estimated volumetric-Computed Tomography dose index and Dose-Length Product values were 40.19 mGy and 2096.60 mGy.cm. In the absence of contrast, the calculated values were 14.65 mGy and 800.40 mGy.cm, respectively. Additionally, for chest Computed Tomography examination, the estimated values were: 12.75 mGy and 423.95 mGy.cm for volumetric-Computed Tomography dose index and Dose-Length Product respectively. These median values represent the proposed diagnostic reference values of the head, chest and abdominal pelvis regions.

The proposed Diagnostic Reference Level are comparable to recommended International Atomic Energy Agency and International Commission Radiation Protection Publication 135 and other regional published data by European Commission and Regional National Diagnostic Reference Level in Africa. These reference levels will serve as benchmarks to guide clinicians in optimizing radiation dose levels while ensuring accurate diagnostic image quality at the facility.

[1] ICRP, Diagnostic reference levels in medical imaging. ICRP Publication 135. Ann. Icrp, 2017. 46(1): p. 1-144.

- [2] Tsapaki, V., Radiation dose optimization in diagnostic and interventional radiology: Current issues and future perspectives. *Physica Medica*, 2020. 79: p. 16-21.
- [3] Menzel, H., H. Schibilla, and D. Teunen, European guidelines on quality criteria for computed tomography. Luxembourg: European Commission, 2000. 16262.
- [4] Kumsa, M.J., et al., Establishment of local diagnostic reference levels for common adult CT examinations: a multicenter survey in Addis Ababa. *BMC Medical Imaging*, 2023. 23(1): p. 6.
- [5] Paulo, G., et al., Diagnostic Reference Levels based on clinical indications in computed tomography: a literature review. *Insights into Imaging*, 2020. 11(1): p. 1-9.
- [6] Uushona, V., et al., Establishment of regional diagnostic reference levels in adult computed tomography for four African Countries: a preliminary survey. *Radiation Protection Dosimetry*, 2022. 198(7): p. 414-422.
- [7] Ahmed, N.A., et al., Proposed national diagnostic reference levels for standard radiographic X-ray procedures in Sudan. *Radiation Protection Dosimetry*, 2020. 190(4): p. 419-426.
- [8] Muhogora, W., et al., Patient doses in CT examinations in 18 countries: initial results from International Atomic Energy Agency projects. *Radiation protection dosimetry*, 2009. 136(2): p. 118-126.
- [9] Salama, D.H., et al., Establishing national diagnostic reference levels (DRLs) for computed tomography in Egypt. *Physica medica*, 2017. 39: p. 16-24.
- [10] Khelassi-Toutaoui, N., et al., Adult CT examinations in Algeria: towards updating national diagnostic reference levels. *Radiation Protection Dosimetry*, 2020. 190(4): p. 364-371.

Combined Optical and CT for operational imaging of small animals

Spectral's Lago and MOLECUBES' X-CUBE have been integrated for bioluminescence, fluorescence, and CT

The Lago Optical CT by Spectral Instruments Imaging is a fully integrated solution that delivers high-performance optical coherence tomography. Combining the Lago in-vivo optical imaging system with the pioneering X-CUBE CT imager by MOLECUBES allows operational imaging of small animals, including bioluminescence, fluorescence imaging, and CT, without compromising the integrity of research outcomes.

The Lago uses a high-performance CCD camera that is air-cooled to -90°C to record luminescent and fluorescent images, which are collected by a large-aperture lens with automated filters and field-of-view selections. Being equipped with a 25 x 25 cm Field-of-View (FOV) that is the largest available allows an unmatched capacity of 10 mice, delivering higher throughput for translational studies that require large sample sizes, including vaccine research and oncology. The Lago's patented LED illumination and weak signal detection provide unprecedented power and previously unattainable sensitivity for fluorescence and bioluminescence.

The X-CUBE allows fast mouse and rat CT imaging at extremely low doses, with excellent soft-tissue contrast and a resolution of up to 50 microns. It achieves enhanced imaging with gated and dynamic contrasts, as well as iterative reconstruction techniques. Intuitive wireless software, combined with multimodal small animal beds, allows for easy and modular imaging. The X-CUBE's imaging unit is self-shielded, making it lightweight and portable, which is ideal for laboratories with limited bench space.



MOLECUBES
MODULAR
BENCHTOP
IMAGING



For further information or to book a demonstration contact:

Southern Scientific Limited
Scientific House, The Henfield Business Park
Shoreham Road, Henfield, BN5 9SL, UK

E-mail: info@southernscientific.co.uk

Tel: +44 (0)1273 497600

www.southernscientific.co.uk



**Southern
Scientific**

EXPERIENCE & EXPERTISE

INTERNET ACCESS DURING THE MEETING

There are two wireless networks available at the venue. 'Eduroam' is a common guest wireless network available at academic institutions. 'The Cloud Network' can be accessed by attendees, who are not affiliated with academia.

HOW TO USE 'EDUROAM'

'Eduroam' is an international service that allows users to connect to a wireless network at participating institutions using the same 'eduroam' network. Visitors from a participating institution can connect to 'eduroam' at King's College London.

HOW TO USE 'THE CLOUD NETWORK'

Anyone visiting King's College London can connect to The Cloud by simply choosing this network on their mobile device. To connect go to your wifi settings on your device, select 'The Cloud' and register if not used before.

PNI TEAM

PNI ORGANISING COMMITTEE

The PNI symposium is a collaborative meeting organised by colleagues from King's College London (KCL), University College London (UCL) and the University of Hull – Hull York Medical School (HYMS).

Please do not hesitate to get in touch throughout the meeting – we are happy to help address any questions you may have.



Dr Gilbert Fruhwirth



Prof Steve Archibald



Dr Louis Allott



Prof Tammy Kalber



Dr Kerstin Sander

ENDORSEMENT AND SPONSORSHIP

ENDORSEMENT

As in recent years, the 5th PNI Symposium is endorsed by the European Society for Molecular Imaging (ESMI). We are grateful for the continuous support by the leading society in this field.



SPONSORS

The PNI symposia would not be possible without the generous support of our sponsors. This year, we have received funding from the following industrial partners:

